Published in final edited form as:
Brain Struct Funct. 2014 March ; 219(2): 719–749. doi:10.1007/s00429-013-0531-9.

Differential distribution of phospholipase C beta isoforms and diaglycerol kinase beta in rodents cerebella corroborates the division of unipolar brush cells into two major subtypes

Gabriella Sekerková[1], **Masahiko Watanabe**[2], **Marco Martina**[3], and **Enrico Mugnaini**[1]

[1]Department of Cellular and Molecular Biology, The Feinberg School of Medicine of Northwestern University, Chicago, IL 60611, USA

[2]Department of Anatomy, Hokkaido University School of Medicine, Sapporo 060-8638 Japan

[3]Department of Physiology, The Feinberg School of Medicine of Northwestern University, Chicago, IL 60611, USA

Abstract

Sublineage diversification of specific neural cell classes occurs in complex as well as simply organized regions of the central and peripheral nervous systems; the significance of the phenomenon, however, remains insufficiently understood. The unipolar brush cells (UBCs) are glutamatergic cerebellar interneurons that occur at high density in vestibulocerebellum. As they are classified into subsets that differ in chemical phenotypes, intrinsic properties, and lobular distribution, they represent a valuable neuronal model to study subclass diversification. In this study we show that cerebellar UBCs of adult rats and mice form two subclasses – type I and type II UBCs - defined by somatodendritic expression of calretinin (CR), mGluR1α, phospholipases PLCβ1 and PLCβ4, and diacylglycerol kinase-beta (DGKβ). We demonstrate that PLCβ1 is associated only with the CR^+ type I UBCs while PLCβ4 and DGKβ are exclusively present in $mGluR1\alpha^+$ type II UBCs. Notably, all $PLC\beta4^+$ UBCs, representing about 2/3 of entire UBC population, also express mGluR1α. Furthermore, our data show that the sum of CR^+ type I UBCs and $mGluR1\alpha^+$ type II UBCs accounts for the entire UBC class identified with Tbr2 immunolabeling. The two UBC subtypes also show a very different albeit somehow overlapping topographical distribution as illustrated by detailed cerebellar maps in this study. Our data not only complement and extend the previous knowledge on the diversity and subclass specificity of the chemical phenotypes within the UBC population but provide a new angle to the understanding of the signaling networks in type I and type II UBCs.

Keywords

calretinin; cochlear nuclei; mGluR1alpha; PLC beta1; PLC beta3; PLC beta4; Purkinje cells; vestibulocerebellum

Introduction

The topological distribution of afferent and efferent connections within a specific brain center is often accompanied by subclass differentiation of its individual neuron lineages and

Corresponding author: Gabriella Sekerkova Feinberg School of Medicine, Northwestern University Department of Cell and Molecular Biology 5-465 Searle bldg. 320 E. Superior str. Chicago, Il 60611 phone :312 503 4301 g-sekerkova@northwestern.edu.

Conflict of interest The authors declare that they have no conflict of interest.

may involve discrete patterns of gene expression that determine diverse membrane properties and signal transduction pathways. The unipolar brush cells (UBCs) represent a unique class of excitatory glutamatergic interneurons that display diverse morphological, chemical and electrical phenotypes, whose significance is still insufficiently understood (Mugnaini et al. 2010; Kim et al. 2012). UBCs are found in the granular layer of the cerebellar cortex and the cochlear nuclear complex, and occur at highest density in regions involved in head and eye movement and orientation to sounds, specifically the vestibulocerebellar lobules and the regions of the cochlear nuclear complex termed “granule cell domains”, including the superficial granular layer (sgl), and dorsal cochlear nucleus (DCN) (Harris et al. 1993; Mugnaini and Floris 1994; Diño and Mugnaini 2008).

UBCs are notable neurons in many ways. Together with the granule cells they represent the excitatory neurons of the cerebellar cortex. Although they are severely outnumbered by granule cells in all lobules in which they occur, the UBCs not only receive mossy fiber inputs like the granule cells, but also provide the granule cells with axo-dendritic and dendro-dendritic excitatory inputs (Mugnaini et al. 2010). The UBCs receive one-to one extrinsic mossy fiber inputs on the dendritic brushes within special glomeruli (Mugnaini et al. 1994; Jaarsma et al. 1996; Diño et al. 2001); the axons of UBCs in turn send outputs to granule cells and other UBCs thus forming an excitatory, intrinsic cerebellar network that has the capacity to synchronize and amplify mossy fiber inputs to potentially large populations of granule cells (Rossi et al. 1995; Diño et al. 2000; Nunzi et al. 2001; Rousseau et al. 2012).

UBCs express a variety of ionotropic and metabotropic receptors, as well as fast- and slow-inactivating voltage-gated calcium channels associated with calcium transients, whose magnitude in the dendritic brush exceeds that in the cell body (Diana et al., 2007; Birnstiel et al., 2009). UBCs were distinguished in subclasses displaying differential -but overlapping- distributions on the basis of the expression of the calcium binding calretinin (CR) and the group I metabotropic glutamate receptor mGluR1α (Nunzi et al. 2002); the major UBC subclass (>65%) consisting of smaller cells (~48 μm^2 soma size in mouse) expresses mGluR1α (mGluR1α$^+$ UBCs) but not CR (CR$^-$ UBCs), whereas a minor subclass (<35%) of slightly larger cells (~63 μm^2 soma size in mouse) are mGluR1α-negative (mGluR1α$^-$ UBCs) and express CR (CR$^+$ UBCs) (Nunzi et al. 2002; Sekerková et al. 2004; Kim et al. 2012). UBCs immunoreactive for both mGluR1α and CR represent but a very small percentage (<3%) of UBCs in the mature cerebellum (Nunzi et al. 2002; Chung et al. 2009a), although they may be slightly more numerous in the cochlear nuclear complex (Diño and Mugnaini 2008).

Nakamura et al. (2004) demonstrated that beta-4 phospholipase C isoform (PLCβ4) is strongly expressed in mGluR1α$^+$ UBCs (mGluR1α$^+$/PLCβ4$^+$ UBCs), while the level of expression in CR$^+$ UBCs appeared low. This observation is in agreement with the notion that mGluR1α activates G protein pathways, which in turn leads to activity of PLCβ isozymes, production of second messengers diacylglycerol and inositol 1,4,5-trisphosphate (IP3) and stimulation of G protein-dependent inward rectifying heteromeric potassium channels (GIRKs), of which GIRK1, GIRK2 and GIRK3 are expressed in UBCs (Knoflach and Kemp 1998; Aguado et al. 2008). Notably, GIRK2 immunoreactivity was reported in CR$^+$ UBCs, but not in mGluR1α$^+$ UBCs (Kim et al. 2012). Most UBCs, furthermore, express the group II metabotropic glutamate receptor mGluR2 (Ohishi et al. 1993a, b; Neki et al. 1996; Jaarsma et al. 1998; Nunzi et al. 2002; Sekerková et al. 2004; Russo et al. 2008).

A recent study revisited the chemical phenotypes of the UBC subclasses by performing cytochemical analysis using an antibody to PLCβ4 paired with either anti-mGluR1α or anti-CR antibodies, and suggested a more complex subclass repartition within the adult, murine,

cerebellar UBC population (Chung et al. 2009a, b). The study proposed an essentially tripartite division, each of the subclasses representing approximately one third of the entire population: one subclass appeared mGluR1α$^+$/PLCβ4$^+$/CR$^-$, a second subclass PLCβ4$^+$/mGluR1α$^-$/CR$^-$, and a third subclass CR$^+$/mGluR1α$^-$/PLCβ4$^-$. Such classification seems to suggest that PLCβ4 and CR expression are mutually exclusive, whereas the expressions of PLCβ4 and mGluR1α are positively linked in only one third of the UBCs. The large subset of PLCβ4$^+$ UBCs lacking expression of both CR and mGluR1α could thus be considered a new, third UBC subclass in which PLC activation would potentially be coupled to G protein-coupled receptors (GPCRs) other than mGluR1α. Additionally, the UBCs expressing CR but not PLCβ4 (CR$^+$/PLCβ4$^-$/mGluR1α$^-$ UBCs) could express other phospholipases of the PLC family. Mammalian PLCs form six enzyme families (PLCβ, γ, δ, ε, δ, ε) with multiple isoforms that contain several conserved domains capable of a variety of ligand binding properties; moreover, topological studies indicate that activity and movement of PLC within the cell is stringently regulated by molecular mechanisms that are progressively becoming understood (Bunney and Katan 2011). Images of phospholipase expression patterns in the Allen Brain Atlas of the mouse cerebellum support the presence of more than one PLC isozyme in cells potentially belonging to the UBC class; while PLCβ4 expression appears most abundant, message for PLCβ1 - but perhaps not PLCβ2, PLCβ3, PLCγ,δ,ε,ε - might also be present in a number of cells (Lein et al. 2007).

In this study we set out to analyze further the expression of mGluR1α and CR in UBCs in combination with antibodies to PLCβ1, PLCβ3, PLCβ4, and diacylglycerol kinase β (DGKβ). We demonstrate that PLCβ1 and PLCβ4 are distinctively co-localized with CR and mGluR1α, respectively, while DGKβ is present exclusively in mGluR1α$^+$ UBCs. We also produced quantitative topographic maps of UBC distribution across cerebellar lobules that show the sum of CR$^+$ UBCs and mGluR1α$^+$ UBCs fully accounts for the cell class that in confocal microscopy is labeled by antibody to the transcription factor eomesodermin (or T-Box brain protein 2, Tbr2), which is considered a *bona fide* UBC population-marker. The new data support the original subdivision of the UBCs in two distinctive – CR$^+$/PLCβ1$^+$ and mGluR1α$^+$/PLCβ4$^+$/DGKβ$^+$ - UBC subclasses, further indicating that the two subclasses are endowed with different signal transduction cascades and may differentially regulate calcium homeostasis.

Materials and Methods

Animals and tissue preparation

This study was carried out on rats and mice in accordance with the guidelines issued by the National Institutes of Health and the Society for Neuroscience, with attention to minimize the number of experimental animals and their suffering. We used adult male rats (Sprague-Dawley; 2-3 months old) and mice (CD1-wild type and Tg(Grp-EGFP)DV197Gsat; 2-3 months old) from colonies bred and housed in the Center for Comparative Medicine *vivarium* at Northwestern University Feinberg School of Medicine. The Tg(Grp-EGFP) mice were generated by the GENSAT project (Doyle et al. 2008). In these transgenic animals the neuronal expression of EGFP is present exclusively in the mGluR1α$^+$ UBCs, and is especially evident in their somata (Kim et al. 2012).

Rats and mice were deeply anesthetized with sodium pentobarbital (60 mg/kg body weight) and then perfused through the ascending aorta with saline followed by 4% freshly prepared formaldehyde in 0.12 M phosphate buffer (PB), pH 7.4. One hour after the perfusion, the brains were dissected out and were either embedded in paraffin or cryoprotected in passages of 10-20-30% sucrose in phosphate buffered saline (PBS) for cryosectioning. Brain embedment and paraffin sectioning were done by AML Laboratories, Inc (Baltimore). Sagittal or coronal cerebellar sections of paraffin embedded blocks were cut at 8 μm,

deparaffinized in xylenes, and rehydrated in descending series of ethyl alcohols. After rinsing in water, sections were then subjected to an effective antigen retrieval protocol, using a pressure cooker with a 1x Rodent Decloacker solution (Biocare Medical) for 20 minutes, followed by a 10 minutes treatment with 0.1% sodium borohydride in Tris-buffered saline (TBS; 100 mM Tris, 150 mM NaCl; pH 7.4). Cryoprotected cerebella were sectioned serially in the sagittal or coronal planes at 24 μm on a freezing-stage microtome and collected in multiwell plates.

Immunohistochemistry

Primary antibodies—The following primary antibodies were used: mouse and rabbit anti-CR, rabbit anti-DGKβ, mouse and rabbit anti-mGluR1α, rabbit anti-PLCβ1, rabbit and guinea pig anti-PLCβ3 rabbit and guinea pig anti-PLCβ4, and chicken anti-Tbr2. Detailed specifications of these antibodies are listed in Table 1. Specificity of antibodies to CR, DGKβ, mGluR1α, and PLCβ4 has been validated previously (Shigemoto et al. 1997; Nunzi et al. 2002; Nakamura et al. 2004; Sarna et al. 2006; Hozumi et al. 2008; Chung et al. 2009a, b; Hozumi et al. 2009). Specificity of Santa Cruz PLCβ1 and PLCβ3 antibodies was validated by Western blot analysis.

Bright-field microscopy—Both paraffin sections and cryosections were processed for immunohistochemistry according to an avidin/biotin amplification protocol. Briefly, the endogenous peroxidase activity was blocked in 0.3% H_2O_2 and 10% methanol in TBS. Unspecific binding was suppressed in a blocking solution containing 5% normal goat serum (NGS) and 1% bovine serum albumin (BSA) in TBS with 0.2% Triton X-100. Sections were then incubated overnight, or up to 2 days at 4°C with primary antibodies. For immunoreactions with rabbit anti-PLCβ1 G-12, guinea pig anti-PLCβ3 (Frontier Institute Co) and rabbit and guinea pig anti-PLCβ4 antibodies, sections were treated with 33% MeOH/67% PBS for 3min, 67% MeOH/33%PBS 3min, 100% MeOH 3min, and then in the reverse gradient for 3min each step (Nomura et al. 2007). Bound antibodies were detected using biotinylated anti-mouse or anti-rabbit IgG (GE Healthcare), ABC Elite kit (Vector) and 3,3”-diaminobenzidine (DAB). Control sections incubated without primary antibodies were free of immunoreaction products.

Immunofluorescence—Sections were incubated with a cocktail of primary antibodies raised in different species. Bound primary antibodies were visualized by secondary antibodies coupled to Alexa 488 or Alexa 594 (Invitrogen). To ascertain whether the sum of the CR^+ and $mGluR1\alpha^+$ UBC subclasses accounts for the entire UBC population we used a mixture of three primary antibodies, anti-Tbr2, anti-CR and anti-mGluR1α. Tbr2 is a marker for all UBC nuclei, while CR and mGluR1α are UBC subclass-specific markers. The Tbr2 binding sites were revealed with Alexa 594-labeled secondary antibody, while binding sites of both CR and mGluR1α were revealed with Alexa 488-labeled secondary antibody.

Western blotting

Protein lysates were prepared from cerebellar lobule X and lobule V. The tissues were homogenized in 5 volumes (ml/g of wet tissue) of RIPA buffer (150mM NaCl, 50mM Tris, pH 8.0; 0.1% SDS, 0.1% Triton X-100, 0.5% sodium deoxycholate) containing proteinase inhibitor cocktail (1 pill/10 ml RIPA buffer; Roche) and centrifuged for 10 min to remove the tissue debris. The supernatants were diluted 3:1 with NuPage LDS Sample buffer (4x; Invitrogen) and heated at 72°C for 10 min. The proteins in the homogenates were separated by NuPage 4-12% Bis-Tris Gel (Invitrogen) and then electroblotted onto nitrocellulose membrane (Trans-Blot Transfer Medium; Bio-Rad). After 1 hr blocking with 10% skim milk in TBS the membranes were incubated with rabbit anti-PLCβ1 G-12 (sc2051; 1:1000) and R-233 (sc-9050;1:500), rabbit anti PLCβ3 C-20 (sc403; 1:500) and H-84 (sc13958;

1:500) or guinea pig anti PLCβ3 (1 μg/ml, Frontier Institute) followed by incubation with secondary antibodies conjugated to horseradish peroxidase (anti rabbit-HRP,1:3000; Promega; anti guinea pig-HRP, 1:5000, Millipore). Immunoreaction was visualized by enhanced chemiluminescence (Yakunin and Hallenbeck 1998).

Image acquisition

Images of cerebellar sections were acquired with a Spot RT CCD video-camera (Diagnostic Instruments) mounted on a Nikon Eclipse E800 microscope. Laser scanning confocal images were obtained with a Nikon PCM 2000 Confocal Microscope System using Simple PCI Program. Images were analyzed individually or in z-stacks of different depths. For co-localization experiments, type FF immersion oil was used with either a 40x plan-fluor lens (numerical aperture 1.3) or a 60x plan-apochromatic lens (numerical aperture 1.4). To minimize channel spillover the images were sequentially acquired. All images were processed with Adobe Photoshop CS3. Brightness and contrast were adjusted.

Quantitative analysis and construction of the UBC distribution maps

The numbers CR^+, $mGluR1\alpha^+$ and $Tbr2^+$ UBCs were counted in sagittal and coronal cerebellar sections of rat and mice. Two to three animals were used for each counting. Based on UBC densities the following regions were defined: regions 1-3 in IXc; regions 1-4 in paraflocculus (regions 1 and 2 were further assigned to ventral paraflocculus); transition zones between lobules III to IV, IX to X, IXa to IXb, and flocculus to paraflocculus; dorsal and ventral leaflet of nodulus; medullary vellum border in nodulus. In some rat specimens the last folium of the uvula is subdivided into IXc and IXd by a shallow sulcus (Larsell 1968); therefore, we labeled regions 2 and 3 as part of IXc/d, especially in coronal sections in which the sulcus between IXc and IXd could not be discern. In the coronal sections the midline of nodulus and uvula was identified and 7 mid-to lateral zone were established on each sides (see Figs. 7, 9). The width of zone 1 (midline zone) was ~60 μm in mice and 100 μm in rat; zones 2-6 were ~230 μm wide in mice and ~250 μm wide in rat. The width of zone 7 was not determined as it represented the most lateral portions of nodulus. UBC numbers were counted for each lobule, region and zone. Tiff images of cerebella were transferred to NIH ImageJ Program (http://rsb.info.nih.gov/ij/), where the area of the cerebellar lobules, regions and zones were outlined using the freehand selection tool. The outlined areas were automatically calculated by the ImageJ program. UBC densities were expressed as number of UBCs/0.01 mm^2. To facilitate visualizing the distribution of the UBCs we constructed a gradient map illustration of the cerebellum using sagittal and coronal section diagrams. In these maps the highest UBC density was considered as 100%, and it is shown in intense red color. The black color, at the other end of the scale was assigned to areas without UBCs (0%).

To determine the coexpression of PLCβ1 and PLCβ4 in CR^+ UBCs or $mGluR1\alpha^+$ UBCs we counted UBC in double labeled cerebellar sections (CR/PLCβ1; CR/PLCβ4; mGluR1α/PLCβ1; mGluR1α/PLCβ4). Large fields of granule cell layer from UBC-rich nodulus and uvula were captured by confocal imaging using 40x plan-fluor immersion oil lens (Nikon). The images labeled with different fluoroprobes were sequentially captured, saved as tiff files and analyzed in Adobe Photoshop. We analyzed 15 randomly chosen fields (N=3 mice or rats), each field contained on average 47 UBCs (19-89 UBCs/field). The immunolabeled UBCs were counted in green (1^{st} antibody) and red (2^{nd} antibody) channels separately and then analyzed in merged red/green channel to assess the colocalization of the antibodies in the same UBC. $CR^+/PLC\beta4^-$ UBCs were counted in a 315×210 mm field mounted on the ocular of a Nikon eclipse microscope. At 40x magnification we could clearly and unequivocally identify CR^+ UBCs and $PLC\beta4^+$ UBCs in fluorescence microscope using either TRITC HYQ or FITC HYQ single-band filters (Nikon). The presence or absence of

double-labeling was checked with a triple band filter D-F-T (Nikon) recognizing signals of DAPI, FITC and Texas red. To avoid the obvious caveats of fluorescence imaging half of these fields were also analyzed by confocal imaging. We did not find any differences in the numbers of single/double-labeled UBCs when the 2 methods of analysis were compared. PLCβ1$^+$ UBC were not quantified in mouse cerebella as we could not unequivocally distinguish them from the labeled granule cells.

The UBCs in the Tbr2/CR/mGluR1α triple-labeled experiments were analyzed by confocal imaging. Large field of nodular and uvular granule cells layer, typically containing ~68 UBC (18-147 UBCs/field), were captured by confocal imaging using 40x plan-fluor immersion oil lens (Nikon). In red channel we identified every Tbr2$^+$ UBC nucleus in the captured field. Tbr2 has been shown as a specific UBC marker, present in most if not all UBCs (Englund et al. 2006; Diño and Mugnaini 2008).To determine whether the Tbr2$^+$ nuclei can be assigned to either CR$^+$ UBCs or mGluR1α$^+$ UBCs (see Fig. 6 and Supplementary Fig. 2) the confocal images were analyzed in combined red and green channel.

Results

To evaluate the quality of immunostaining of sections of rat and mouse cerebella were labeled with antibodies to PLCβ1, PLCβ3, or PLCβ4 using DAB as the chromogen and observed by bright field microscopy. Specificity of the Santa Cruz G12 (sc205) and R233 (sc9050) PLCβ1 antibodies was assessed in immunoblots and by immunolabeling patterns in whole brain sections. Specificity of the guinea pig anti-PLCβ3 and PLCβ4 antibodies has been validated previously (Nakamura et al. 2004; Sarna et al. 2006; Nomura et al. 2007), and was further assessed in brain sections. Western blot analysis performed on tissue obtained from rat and mouse cerebellar lobules V and X using both PLCβ1 antibodies detected a single band corresponding to a ~145-150 kDa protein (Fig. 1a) that matched the predicted molecular weight of the PLCβ1 (Fukaya et al. 2008). Each of the three PLCβ isozymes showed a distinctive subtype-specific pattern of immunolocalization in cerebellum, as previously reported (Tanaka and Kondo 1994; Roustan et al. 1995; Watanabe et al. 1998; Hashimoto et al. 2001; Vitale et al. 2004; Sarna et al. 2006; Nomura et al. 2007; Fukaya et al. 2008; Chung et al. 2009a). Moreover, we observed novel aspects of PLCβ expression in UBCs and Purkinje cells. PLCβ1 and PLCβ4 antibodies labeled subclasses of both Purkinje cells and UBCs, while PLCβ3 immunoreactivity only marked a subset of Purkinje cells, but not UBCs. Expression of PLCβ isoforms in different cerebellar neurons is summarized in Table 2.

PLCβ1 immunostaining

Overall, PLCβ1 immunostaining of the brainstem and cerebellum was less pronounced than in the forebrain in both mouse and rat (rat shown in Fig. 1b). Interestingly, the two PLCβ1 antibodies (Santa Cruz sc205 and sc9050) displayed a degree of species specificity: G-12 (sc205) provided more distinct immunolabeling in rat tissue than in mouse tissue, while R233 (sc9050) worked better in the mouse. The immunoreactivity of Purkinje cell bodies and dendrites dominated the picture throughout all cerebellar lobules in both rat and mouse; in both species UBCs were stained, while Golgi and Lugaro cells were PLCβ1 immunonegative. Species differences in immunostaining were notable as reported below.

Rat—PLCβ1 antibody distinctly labeled UBCs in the vestibulocerebellum (Figs. 1c, d, f, f', 2b-d), and specifically in nodulus, regions 2 and 3 of IXc, flocculus, and region I of ventral paraflocculus, as well as in the DCN and sgl of the cochlear nuclear complex (Fig. 1f, f"). UBC somata and dendritic brushes were intensely stained (Fig. 1d, f', f") and stood out even

at low magnification (Fig. 1c, f). The transition zones between the nodulus and uvula (black dashed line in Fig. 1c) and the flocculus and paraflocculus, the latter including part of region 1 of ventral paraflocculus (black dashed line in Fig.1f), contained particularly dense PLCβ1$^+$ UBC population. In coronal sections the PLCβ1$^+$ UBCs showed a nearly uniform distribution in nodulus, with slightly more UBCs close to midline (Fig. 2b, c). In region 3 of IXc/d three bands of high density PLCβ1$^+$ UBCs were seen (Fig. 2b, c), one at the midline and two lateral bands (one on each side). In region 2 of IXc/d, however, the bands dissipated and the UBC were mostly concentrated in the midline zone (not shown). PLCβ1$^+$ UBCs were mostly absent from other cerebellar lobules, including the rest of the uvula and paraflocculus. PLCβ1 immunolabeled granule cells were present throughout the granular layer (Figs. 1c, d, f, 2b-d).

The Purkinje cell bodies and their primary dendrites were stained at background level (Figs. 1c-f, 2b-d). In the upper 2/3^{rds} of the molecular layer, however, a proximal-to-distal gradient of immunolabeling was present that would appear consistent with increasing immunoreactivity of the peripheral Purkinje dendritic branches (Figs. 1c, e, f, 2b-d). The somata of molecular layer interneurons and the pinceaux surrounding the initial segment of the Purkinje cell axons were moderately immunopositive (Fig. 1e). In the cerebellar nuclei, the neuropil was diffusely immunoreactive (Fig. 1f), whereas neuronal cell bodies were unstained, with the exception of faintly immunolabeled, scattered small cells (not shown). In the DCN, the dendrites of cartwheel neurons, the microcircuit equivalent of Purkinje cells (Mugnaini et al. 1987; Berrebi et al. 1990; Berrebi and Mugnaini 1991), were intensely stained (asterisks in Fig. 1f).

Mouse—PLCβ1$^+$ UBCs were best visualized in paraffin sections after intense antigen retrieval (Fig. 3a). By contrast, in standard cerebellar cryosections PLCβ1$^+$ UBCs barely stood out from the PLCβ1$^+$ granule cells, especially at low magnification (Fig. 3d, e). Both the UBC somata and their dendrites ending in a brush-like tip were immunolabeled (Fig. 3b). Like in rat, the distribution of PLCβ1$^+$ UBCs was restricted to the vestibulocerebellum including the nodulus (Fig. 3a, d), region 2 of IXc in uvula (Fig. 3d), flocculus and region 1 of ventral paraflocculus (not shown). PLCβ1$^+$ UBC were rare in other cerebellar lobules (Fig. 3d, e). The highest PLCβ1$^+$ UBC density was seen at the transition zones nodulus to uvula (Fig. 3a) and flocculus to paraflocculus; the latter included parts of region 1 of ventral paraflocculus and flocculus (not shown). In coronal sections the midline regions of the nodulus dorsal leaflet and region 2 of IXc displayed densely packed PLCβ1$^+$ UBCs (Fig. 3d). In region 2 of IXc three bands with densely packed PLCβ1$^+$ UBCs were distinguishable (Fig. 3d), one medial band and two lateral bands. PLCβ1$^+$ UBCs were present in the DCN (not shown), albeit they were hard to discern from the stained neuropil.

Although all Purkinje cells were immunostained over the entire somatodendritic compartment, there were remarkable parasagittal stripes of Purkinje cells that stood out from their neighbors (Fig. 3d, and Supplementary Fig. 1a, b). The molecular layer interneurons (basket and stellate cells) also presented a moderate cytoplasmic staining in cell bodies and stem dendrites; furthermore, the pinceaux were markedly immunostained throughout the cortex (Fig. 3c). Both folial and deep white matter were unstained (Fig. 3d, e); in the cerebellar nuclei the neuropil was diffusely immunoreactive (Supplementary Fig. 1a), whereas neuronal cell bodies were at best barely above background (not shown). In the DCN, the somata and dendrites of cartwheel cell showed intense PLCβ1 immunostaining (Supplementary Fig. 1a).

PLCβ3 immunostaining

We have tested 3 different PLCβ3 antibodies; guinea pig anti-PLCβ3 from Frontier Institute and 2 rabbit anti-PLCβ3 (C-20 and H-84) from Santa Cruz. In mouse cerebella only the antibody purchased from Frontier Institute produced reliable and specific immunostaining of the Purkinje cells (Fig. 3f, g and Supplementary Fig. 1c, d). In rat all 3 antibodies showed insufficient/faint immunolabeling of the Purkinje cells (Fig. 2e), and therefore are considered but briefly. In both species however, all other neuron types, including the UBCs, were immunonegative, as previously described (Sarna et al. 2006; Nomura et al. 2007).

Rat—PLCβ3 immunostaining with antibody raised against mouse PLCβ3 (Frontier Institute) even though faint, was restricted to Purkinje cell bodies distributed in bands of predominantly parasagittal distribution; the Purkinje cell dendritic arbors were unstained (Fig. 2e). The PLCβ3 C-20 antibody raised against rat PLCβ3 also showed inadequate Purkinje cell labeling but on the other hand intensely labeled the climbing fibers and the mossy fibers; the later especially in nodulus and flocculus (not shown). Further studies are needed to determine the specificity of this peculiar immunolabeling.

Mouse—Overall, Purkinje cell immunoreactivity was higher in the posterior lobe, including the flocculus, paraflocculus, nodulus and uvula, than in the anterior lobe (not shown). PLCβ3^{+} Purkinje cells were distributed in parasagittallly orientated stripes (Fig. 3f, g and Supplementary Fig. 1c, d). Notably, the intensity of immunostaining varied in PLCβ3^{+} stripes from intense, to moderate, to faint; the faint degree of staining was barely above background, and therefore might be regarded as characterizing PLCβ3^{-} Purkinje cell off-bands. In the folial white matter immunostaining was restricted to bands of Purkinje cell axons, which extended into the cerebellar nuclei (Supplementary Fig. 1c). In the latter, neurons were immunonegative and the neuropil showed immunostained patches, presumably containing the terminals of PLCβ3^{+} axons. The cartwheel neurons in the DCN were PLCβ3^{-} (Supplementary Fig. 1c).

PLCβ4 immunostaining

The patterns of PLCβ4-immunoreactivity appeared similar in mouse and rat with respect to two most notable aspects: i/ the well-known parasagittal stripes of PLCβ4^{+} and PLCβ4^{-} Purkinje cell somato-dendritic compartments (Figs. 2f-h, 3h-j, 4a-c, e, f, 5a-d, f and Supplementary Fig. 1e, f); and ii/ the distinct immunostaining of UBCs in the granular layer (Figs. 2f-h, 3h-j, 4a-d, f, 5a-e, g). Granule cells were PLCβ4^{+}, but showed only faint to moderate immunolabeling (Figs. 4, 5). Stellate, basket, and Golgi cells were unstained or at background level (Figs. 4b, d-f, 5b, d-f). In the cerebellar nuclei the neuropil was diffusely immunoreactive and the cell bodies and dendrites of small neurons were distinctly stained (Figs. 4f, 5d); the large neurons were at background level. PLCβ4-immunoreactivy was generally cytoplasmic, whereas cell nuclei were unstained. Comparison of rat and mouse sections showed that in every cortical folium in which UBCs occurred, all PLCβ4^{+} UBCs showed distinct immunoreaction signal, thus establishing the PLCβ4 as an excellent UBC subtype specific marker.

Rat—PLCβ4^{+} UBCs (Fig. 4d, g) were enriched in the vestibulocerebellum, throughout which they showed a much more widespread distribution than the PLCβ1^{+} UBCs (compare Figs. 1c and 2b-d with Figs. 4b and 2f-h, respectively). High densities of PLCβ4^{+} UBCs were found not only in nodulus, regions 2 and 3 of IXc, flocculus, and region 1 of ventral paraflocculus but also in IXb, region 1 of IXc, and region 2 of ventral paraflocculus (Figs. 2f-h, 4a-d, f, g). The ventral leaflet of nodulus (Figs. 2f, g, 4b) and the region 1 of ventral paraflocculus contained the highest density of PLCβ4^{+} UBCs. Intriguingly, the dorsal leaflet of nodulus showed much lower UBC density than the ventral leaflet, especially in anterior

coronal sections (see Fig. 2f, but also Fig. 4b). Three high-density bands of PLCβ4$^+$ UBCs in region 3 of IXc/d were discernible at the same location where the high density PLCβ1$^+$ UBC bands were found (in Fig. 2 compare panels f, g to b, c, respectively). Notably, a distinct area between folia IXa and IXb showed marked decline in UBC density, especially when compared to the surrounding areas (asterisks in Fig. 4b). PLCβ4$^+$ UBCs were scattered in other vermal lobules, specifically in I, VI-IXa (Figs. 2f-h, 4a-c), and were also found in the hemispheral lobules (Fig. 4c) and in the rest of paraflocculus (Fig. 4f). The DCN and sgl also contained PLCβ4 immunostained UBC (Fig. 4f, h), albeit the immunostaining was tenuous; the dendrites of cartwheel neurons were faintly immunolabeled.

Mouse—PLCβ4$^+$ UBCs were clearly recognizable by their distinctively stained somata and brushes (Fig. 5e, g). The density of PLCβ4$^+$ UBCs was particularly high in nodulus, IXb, regions 1 and 2 of IXc (Figs. 3h-j, 5a-c, e), flocculus and region 1 of ventral paraflocculus (Fig. 5d, g and Supplementary Fig. 1e, f). Other vermal lobules (I-III, VIb-IXa), the hemispheral lobules and the rest of the paraflocculus also contained scattered PLCβ4$^+$ UBCs (Figs. 3h-j, 5a-d). The highest densities of the PLCβ4$^+$ UBCS were observed in the transition zone nodulus to uvula (Fig. 5b), in the ventral leaflet of the nodulus (Fig. 3j), and in the transition zone flocculus to paraflocculus; the latter included the region 1 of ventral paraflocculus and a portion of the flocculus (Fig. 5d). In coronal sections the midline region of nodulus appeared to contain dense clusters of PLCβ4$^+$ UBCs, while in region 2 of IXc three high density bands of PLCβ4$^+$ UBCs were observed (Fig. 3h, j); one particularly dense band at the midline and two lateral ones. Like in rat, we observed a special UBC-poor area between IXa and IXb (asterisks in Fig. 5b); in mouse, however, this region was completely devoid of UBCs. Numerous PLCβ4$^+$ UBCs were seen in DCN and sgl (Fig. 5d, h and Supplementary Fig. 1e) and the dendrites of the cartwheel neurons showed moderate immunoreactivity.

Cell subclass-specificity of PLCβ1 and PLCβ4 immunostaining

While several cell markers reveal the UBC population in its entirety, other proteins clearly indicate the existence of a distinct phenotypic heterogeneity. Tbr2 is a specific UBC population-marker in developing and adult animals (Englund et al. 2006; Diño and Mugnaini 2008), whereas distinct UBC subpopulations were classified based on CR and mGluR1α expression (Nunzi et al. 2002). A recent study classified UBCs into 3 major subclasses: CR$^+$/mGluR1α$^-$/PLCβ4$^-$, mGluR1α$^+$/PLCβ4$^+$/CR$^-$, and PLCβ4$^+$/mGluR1α$^-$/CR$^-$ (Chung et al. 2009a, b).

To validate this tripartite subdivision, at first we labeled mouse and rat cerebellar tissues with a cocktail of Tbr2, mGluR1α, and CR antisera (Fig. 6 and Supplementary Fig. 2). All three antibodies were previously tested by immunostaining and were proven to be excellent UBC markers. We used Alexa 594-labeled secondary antibody for Tbr2 detection, and Alexa 488 labeled secondaries for the combined visualization of mGluR1α and CR (Fig. 6 and Supplementary Fig. 2). We captured confocal images (40x) of large fields containing numerous UBCs (Fig. 6 and Supplementary Fig. 2) and analyzed each Tbr2$^+$ UBC for double immunolabeling (Fig. 6b-b”, c-c” and Supplementary Fig. 2b-b”, c-c”). We counted 892 (N=2 rats)/1206 (N=3 mice) of Tbr2$^+$ UBCs from nodulus and uvula in both mouse and rat and found that all Tbr2$^+$ UBCs were associated with either mGluR1α or CR. In rat 64% and in the mouse 63% of the Tbr2$^+$ UBCs were immunolabeled with mGluR1α while the remaining Tbr2$^+$ UBCs expressed CR. As expected, both the CR$^+$ UBCs and the mGluR1α$^+$ UBCs were Tbr2$^+$.

As a further control, we also analyzed the UBC density in neighboring 25 μm-thick, DAB-stained sections individually immunoreacted with Tbr2, CR, or mGluR1α (Table 3). In both

rat and mouse the nodulus contained the highest UBC densities irrespective of UBC subtype. The sum of CR^+ UBC and $mGluR1\alpha^+$ UBCs turned out to be roughly equal to the number of $Tbr2^+$ UBCs.

Next, we revisited the distributions of the CR^+ UBCs and mGluR1α UBC subsets in rat and mouse and compared them with the distributions of $PLC\beta1^+$ UBCs and $PLC\beta4^+$ UBCs. We constructed quantitative maps of the densities of CR^+ UBCs and $mGluR1\alpha^+$ UBCs in the cerebellum of rat and mouse and projected these as color gradient maps on sagittal and coronal diagrams of the mouse cerebellum to facilitate reference (Figs. 7-10; numerical data with standard derivation are shown in Supplementary Tables 1-3). The quantitative, topographic analysis underlying these maps is presented in detail as Supplementary Text 1. Briefly, in both rodents the two UBC subsets showed partly overlapping distribution patterns in vestibulocerebellum, but the CR^+ UBC subset was mostly restricted to nodulus and ventral uvula (regions 2 and 3 of IXc/d in rat and region 2 of IXc in mouse). When the gradient maps of CR^+ UBCs and $mGluR1\alpha^+$ UBCs were compared with the distributions of UBCs expressing either PLCβ1 or PLCβ4 it become evident that the two PLCβ antibodies recognized two different UBC subsets. The distribution of $PLC\beta1^+$ UBCs was in register with that of the CR^+ UBCs in both rat (compare Figs. 1c, f, 2b with Figs. 8b, f, 7d-right side, respectively) and mouse (compare Figs. 3a, d with Figs. 10b, 9d-right side, respectively). On the other hand the distribution of $PLC\beta4^+$ UBCs mirrored the distribution of the $mGluR1\alpha^+$ UBCs in both species (for rat compare Figs. 4b, f, 2f with Figs. 8a, e, 7d-left side; for mouse compare Figs. 5b, d, 3j with Figs. 10a, e, 9d-left side).

We then used confocal imaging to ascertain that the two PLCβ isoforms were indeed expressed in two different UBC subsets. In both mouse and rat the $PLC\beta1^+$ UBCs were associated with CR immunostaining (Fig. 11a-f). We analyzed 361 (N=3 rats)/272 (N=3 mice) CR^+ UBCs and 274 (N=3 rats) $PLC\beta1^+$ UBCs and found that all CR^+ UBC were also $PLC\beta1^+$; in reverse all $PLC\beta1^+$ UBCs were CR^+. The $mGluR1\alpha^+$ UBCs were $PLC\beta1^-$ (Fig. 11g-i).

The $PLC\beta4^+$ UBC were immunostained with mGluR1α (Fig. 12a-f). We analyzed 662 (N=3 rats)/835 (N=3 mice) $mGluR1\alpha^+$ UBCs and 496 (N=3 rats)/632 (N=3 mice) $PLC\beta4^+$ UBCs and found that all $PLC\beta4^+$ UBCs were immunolabeled with mGluR1α antibody. In reverse 95% (rat)/ 97% (mice) of the $mGluR1\alpha^+$ UBCs were colabeled with PLCβ4 antibody, albeit a subset of these double labeled UBCs (20% in rat and 21% in mice) showed only a faint PLCβ4 immunostaining, barely above the background level. On the contrary CR^+ UBCs were $PLC\beta4^-$ (Fig. 12g-i). We analyzed 222 (N=3 rats)/220 (N=3 mice) CR^+ UBCs and 413 (N=3 rats)/472 (N=3 mice) $PLC\beta4^+$ UBCs, but none of these cells were double labeled with PLCβ4 or CR, respectively.

DGKβ immunostaining and the UBCs

Immunoreactivity to rabbit anti-DGKβ in the cerebellar cortex differed in cryostat sections and paraffin sections. In cryostat sections immunostaining was restricted to the somatodendritic and axonal compartments of a subpopulation of Purkinje cells. The $DGK\beta^+$ Purkinje cells showed a banded distribution that was especially evident in the posterior cerebellum (not shown).The other cortical neurons, including the UBCs, were unstained. In paraffin sections subjected to rigorous antigen retrieval, however, the DGKβ antibody immunolabeled granular layer cells with typical UBC morphology. UBC somata and brushes were distinctly immunoreactive, albeit variations in the staining intensity of the brushes were apparent (Fig. 13b,d). Notably, the Purkinje cell labeling was attenuated (Fig. 13) compared to cryostat sections. In both species the $DGK\beta^+$ UBCs matched the $mGluR1\alpha^+$/$PLC\beta4^+$ UBCs in the pattern of lobular distribution (for rat compare Figs. 13a to 4b and 8a; for mice compare Figs. 13c to 5b and 10a). Indeed, $DGK\beta^+$ UBCs were present

in virtually all lobules of the cerebellum, but the highest densities were found in nodulus and regions 1-3 (rat)/1-2 (mouse) of IXc (Fig. 13a, c). Flocculus and region 1 of ventral paraflocculus also contained high densities of DGKβ$^+$ UBCs (not shown). The peculiar uvular area marked by extremely low density or absence of either CR$^+$ UBCs or mGluR1α$^+$ UBCs in rat and mouse were clearly recognizable (asterisks in Fig. 13a, c). The DCN and the sgl also contained DGKβ$^+$ UBC, while all of the cartwheel neurons were unstained, in contrast to the banded immunostaining of Purkinje cells

To determine the subclass identity of DGKβ$^+$ UBCs we resorted to confocal imaging. All DGKβ$^+$ UBC showed distinctive mGluR1α immunolabeling (Fig. 14a-f) and were CR$^-$ (Fig. 14g-i). Correspondingly, none of the CR$^+$ UBC were DGKβ$^+$ (Fig. 14g-i). Unexpectedly, however, not all mGluR1α$^+$ UBCs were DGKβ$^+$ (Fig. 14a-f). The intensity of the DGKβ immunolabeling in the mGluR1α$^+$ UBC brushes varied; many brushes were intensely stained, while few showed only moderate-to-faint DGKβ labeling. Some mGluR1α$^+$ UBC brushes were devoid of any DGKβ immunoreactivity. Further experiments are needed to determine whether the lack of DGKβ staining in a small fraction of mGluR1α$^+$ UBCs depends on the molecular form of the enzyme recognized by the specific antibody utilized in this study.

Expression of the PLCβ isoforms in UBC subpopulations and their relation to Purkinje cells stripes

In addition to the patterns of terminations of primary and secondary vestibular fibers (Mugnaini et al. 2010), deployment of UBC subclasses in the cerebellar cortex might be more or less strictly related to the formation of early Purkinje cell maps (Chung et al. 2009a, b). To investigate the possibility that UBC distribution is related to diversification of Purkinje cell phenotype we analyzed the distribution of the two major UBC subtypes - CR$^+$/PLCβ1$^+$ UBCs and mGluR1α$^+$/PLCβ4$^+$ UBCs - in relation to Purkinje cell stripes labeled with antibodies raised against PLCβ1, PLCβ3, and PLCβ4. Immunolabeling with each of the three individual PLCβ antibodies revealed distinct patterns of alternating parasagittal stripes in the Purkinje cells. The intensity of immunolabeling varied in the Purkinje cell stripes; for simplicity three categories of stripes were distinguished; intense, moderate, and faint/negative stripes. PLCβ1$^+$ stripes had not been recognized previously with a proprietary antibody (Fukaya et al. 2008), but recently they were shown with commercial PLCβ1 antibodies (Montaña et al. 2012). Stripes of PLCβ3$^+$ and PLCβ4$^+$ Purkinje cells had been described in detail in the mouse cerebellum. In general, PLCβ3 and PLCβ4 antibodies showed complementary Purkinje cell immunolabeling (see also Sarna et al. 2006; Nomura et al. 2007) in most cerebellar lobules with the notable exception of nodulus, regions 2 and 3 of IXc, flocculus and paraflocculus. A short description of PLCβ1, PLCβ3, and PLCβ4 immunolabeling in Purkinje cell stripes follows with special emphasis on the vestibulocerebellum.

PLCβ1—In the mouse, parasagittally oriented bands of PLCβ1$^+$ Purkinje cells showed either intense or moderate PLCb1 immunoreaction, which resulted in a distinct striped pattern in the molecular layer (Supplementary Fig. 1a, b). In the anterior cerebellum the distribution of the PLCβ1$^+$ Purkinje cell stripes bore similarities with the distribution of the PLCβ3$^+$ stripes, whereas the Purkinje dendritic staining appeared nearly homogeneous in the posterior cerebellum. In region 1 and 2 of IXc five moderately stained stripes interposed between wide, intensely stained Purkinje cell bands were identifiable: one stripe in the midline, and two lateral ones on each side (arrowheads in Fig. 3d, e). Remarkably these stripes were located at the same position as were the PLCβ4$^-$ Purkinje cell stripes in a neighboring section (in Fig. 3 compare panels d, e with panels h, i, respectively). Purkinje cells in the nodulus also showed some degree of variation in immunolabeling (Fig. 3d), with

the clearest, intensely PLCβ1^{+} lateral stripes in the dorsal leaflet of nodulus near the transition between X and IXc (crossed arrow in Fig. 3d). In the flocculus and paraflocculus the Purkinje cells were moderately immunolabeled, with the exception of the anterior parts of the flocculus and region 1 of ventral paraflocculus. In these two structures the Purkinje cells were intensely stained, especially when compared to other Purkinje cells in the paraflocculus (Supplementary Fig. 1a, b). This staining pattern of flocculus and paraflocculus was similar to the staining pattern observed with PLCβ4 antibody (see Fig. 5d and Supplementary Fig. 1a, b, d). Further detailed study is needed to characterize the PLCβ1^{+} Purkinje cell stripes and to elucidate their relation to other well studied Purkinje cell subtype-specific markers (e.g. zebrins). In the rat the PLCβ1antibodies showed only partial Purkinje cell labeling in the proximal dendrites; albeit the staining was uniform throughout the cerebellar cortex (Figs. 1c, f, 2b-d).

PLCβ3—The stripes the PLCβ3^{+} Purkinje cells in the mouse nodulus, region 2 of IXc, flocculus, and paraflocculus (Fig. 3f and Supplementary Fig. 1c, d) differed from PLCβ1 (Fig. 3d and Supplementary Fig. 1a, b) and PLCβ4 (Figs. 3h, 5d and Supplementary Fig. 1e, f) with respect to their width and distribution. In nodulus and region 1 of IXc, most of the Purkinje cells were only moderately stained, while other showed faint/negative immunolabeling (Fig. 3f). Three faint/negative PLCβ3 stripes were present in the nodulus; 1 wide stripe at the midline and 2 lateral stripes one on each side. Notably, these stripes appeared to continue from the ventral to the dorsal leaflets (arrows in Fig. 3f). In region 2 of IXc the striped pattern was not clear, although some of the Purkinje cells showed very little or no labeling. The staining intensity of the Purkinje cells increased in region 1 of IXc, and in the rest of uvula. In these regions the Purkinje cell PLCβ3^{+} stripes corresponded in their distribution pattern to the PLCβ4^{-} Purkinje cell stripes (in Fig. 3 compare panels f, g to h, i respectively), although in reverse (PLCβ3^{-} stripes were PLCβ4^{+} and vice versa). In flocculus and paraflocculus the Purkinje cells were intensely stained, with exception of three moderate to faint/negative patches; one roughly in the area of region 1 and 2 of ventral paraflocculus, the second patch in the ventral portion of paraflocculus, and third in dorsal paraflocculus, near the parafloccular fissure (Supplementary Fig. 1c). In rat sections PLCβ3 immunostaining was inadequate, and therefore we could not credibly evaluate the on/off Purkinje cell stripe pattern.

PLCβ4—In mouse PLCβ4 immunostaining produced a distinct, predominantly parasagittal pattern of alternating Purkinje cell bands in all cerebellar lobules but not in nodulus and flocculus/paraflocculus. In these regions the Purkinje cells were mainly PLCb4^{-} (Figs. 3h, j, 5c, d and Supplementary Fig. 1e, f), although some moderately immunolabeled Purkinje cell bands were discernible in the dorsal leaflet of the nodulus (Fig. 3h, j) and in the anterior portion of the flocculus and region 1 of paraflocculus (Supplementary Fig. 1f). Alternating stripes with intense, moderate and fain/negative PLCβ4 immunostaining were easily distinguishable in the rest of the uvula, including the regions 1 and 2 of IXc (Fig. 3h-j).

In rat the pattern of the Purkinje cell stripes was similar to those observed in mouse, with minor differences. Like in mouse, the molecular layer of the ventral leaflet of the nodulus was immunonegative (Figs. 2f, g, 4a-c), while few moderate to faint patches of Purkinje cell were seen in the dorsal leaflet. In region 3 of IXc/d and the rest of the uvula on/off stripes were easily distinguishable; these stripes were comparable to the stripes observed in mouse. The main difference between the two species was found in paraflocculus, where several patches of moderately labeled Purkinje cells were found interspersed between faint/negative stripes (Fig. 4f), especially in the dorsal paraflocculus (Fig. 4f). The flocculus, however, showed similar distribution of the PLCβ4 immunoreactivity in rat and mouse, i.e., moderately stained anterior portion and negative Purkinje cells in posterior regions.

PLCβ isoform-specific immunostaining and UBCs—As described above the distribution of the three different PLCβ isoforms varied greatly in the vestibulocerebellum. Although some regions showed similarities with respect to the location of the on/off Purkinje cell stripes, the overall immunostaining pattern could be conceived as unique for each of the PLCβ isoforms. In general, we found only scarce correlation between the pattern of PLCβ1, PLCβ3, and PLCβ4 immunostaining in Purkinje cells and UBC distribution (see Figs. 2, 3). In general, rather than being distributed in stripes like Purkinje cells, the UBCs were distributed in zonal fashion, with dense UBC patches/zones near the vermal midline and at the flocculus/paraflocculus transition that includes the region1 of ventral paraflocculus (see also Figs.7-10). An exception seems to be region 2 of lobule IXc/d(rat)/ IXc(mouse), in which clear PLCβ1 and PLCβ4 Purkinje cell stripes and high-density UBC bands were observed (Figs. 2b, c, f, g, 3d, h but also see Figs. 7, 9). Remarkably, both UBC subclasses - CR^+/$PLC\beta1^+$ UBCs and $mGluR1\alpha^+$/$PLC\beta4^+$ UBCs – aggregated in these high-density patches, especially in the band at the midline (Fig. 7, 9). The two lateral UBC bands (one on each side) were roughly positioned below $PLC\beta4^-$ Purkinje cell stripes (these stripes were also moderately immunolabeled with PLCβ1), while the midline UBC band was positioned below both $PLC\beta4^-$ and $PLC\beta4^+$ stripes, the later perhaps as a result of the narrowness of the midline $PLC\beta4^-$ stripe.

Discussion

This immunocytochemical study indicates that cerebellar UBCs of adult rat and mouse express PLCβ1 and PLCβ4, but lack PLCβ3. It appears that PLCβ1 and PLCβ4 are expressed differentially in subclasses of UBCs; whereas the former is co-localized with CR in a smaller subset of UBCs, the latter is co-localized in all the mGluR1α-approximately 2/3 of the entire UBC class. Our data also shows that most if not all $mGluR1\alpha^+$ UBCs are endowed with the PLCβ4 isozyme and in reverse all $PLC\beta4^+$ UBCs express mGluR1α. Thus our data supports the originally proposed separation of the UBCs into two chemically distinct subclasses (Nunzi et al. 2002); type I UBCs expressing CR and PLCβ1 and type II UBCs expressing mGluR1α and PLCβ4.

The differential expression of PLCβ1 and PLCβ4 in type I and type II UBCs likely correlates with their expression of group I and group II mGluR subtypes, which couple to PLC activation primarily via Gq/11 and Gi/o-GS, respectively (Pin and Duvoisin 1995; Nakamura et al. 2004; Tateyama and Kubo 2011). In this study we also detected the presence of DGKβ in UBCs, but only in the type II UBC that express mGluR1α and PLCβ4. DGKβ is suggested to be involved in mGluR5-PLCβ1-DGKβ signaling cascade in the striatal projection neurons (Hozumi and Goto 2012), however in type II UBCs it appears to be associated with mGluR1α-PLCβ4 transduction pathway.

The results of the present study reinforce the notion that intrinsic membrane properties, responses to neurotransmitters, and signal transduction pathways linked to plasma membrane are all consistent with the classification of UBCs in two major subclasses, probably performing different tasks (Mugnaini et al. 2010; Kim et al. 2012; Rousseau et al. 2012).

PLCβ isoforms are expressed in the cerebellum in a cell-subtype specific manner

While PLCβ4 immunoreactivity in cerebellar UBCs had been shown previously, the demonstration of PLCβ1 immunoreactivity in UBCs represents a novel finding. Previous reports indicated that mRNA signal for PLCβ1 is low in the mouse cerebellum, and protein is associated primarily with molecular layer inhibitory interneurons and to a lesser extent with Purkinje cells and granule cells (Sugiyama et al. 1999; Fukaya et al. 2008).

Nakamura et al. (2004) reported intense PLCβ4 immunoreactivity in mGluR1α$^+$ UBCs, which supports our data. The finding that all mGluR1α$^+$ UBCs express the PLCβ4 isoform in mature rodents is, however, in contrast with a recent study suggesting the presence of equal percentages of PLCβ4$^+$ UBCs that are either mGluR1α$^+$ or mGluR1α$^-$ (Chung et al. 2009a, b). As UBCs chemical phenotypes may parallel diverse information transfer from their inputs (Kim et al. 2012), the repartition of UBCs into two, three or more subsets is meaningful for future studies directed to establish whether UBC subclasses are differentially innervated by primary or secondary vestibular fibers and possibly other cerebellar afferents (Mugnaini et al. 2010). The study of Chung et al. (2009a) and the present report, however, are in agreement concerning the density of PLCβ4$^+$ UBCs, which is roughly twice that of the CR$^+$ UBCs. The discordance between the two papers, therefore, rests primarily on the actual density of mGluR1α$^+$ UBCs, which with our protocol is approximately equal to the sum of PLCβ4$^+$/mGluR1α$^+$/CR$^-$ and PLCβ4$^+$/mGluR1α$^-$/CR$^-$ UBCs reported by Chung et al. (2009a). This discrepancy may arise from using different lots of mGluR1α antibodies but also from the efficiency of the membrane permeabilization. We used three different mGluR1α antibodies with the same outcome, that is colocalization of mGluR1α in every PLCβ4$^+$ type II UBC. Our sections were incubated with the primary antibodies diluted in 1%NGS/1%BSA/TBS solution containing 0.2% Triton-X 100 for at least 2-3 days. However in the previous study only 0.1% Triton-X 100 was used for 16-18 hours (Chung et al. 2009a). Therefore it is conceivable that the mGluR1α antibodies in our study penetrate into the sections well enough to label the entire subclass of PLCβ4 expressing UBCs. Concerning the small percentage of UBCs expressing a mixed phenotype PLCβ4$^+$/mGluR1α$^+$/CR$^+$ (Chung et al. 2009a) or CR$^+$/mGluR1α$^+$ (Diño and Mugnaini 2008), closer evaluation may require additional information on their specific inputs. Notably, UBCs co-expressing CR and mGluR1α are more frequent in the cerebella of young animals (P22-P24), although they represent only ~3-5% of all UBCs (Kim et al. 2012). Taken together, our results indicate that two major subclasses of UBCs, one of which is CR$^+$/mGluR1α$^-$ (type I UBCs) and the other mGluR1α$^+$/CR$^-$ (type II UBCs), express two distinct isoforms of the PLCβ family of enzymes, PLCβ1 and PLCβ4, respectively.

A differential expression of PLCβ isoforms in distinct neuronal subsets is not unprecedented, as differences in the distribution of PLCβ isozymes in the Purkinje cells have been previously reported (Sarna et al. 2006; Nomura et al. 2007). The data presented in this study complement the earlier immunocytochemical studies by demonstrating varying degrees of immunoreactivities for PLCβ3 and PLCβ4 in Purkinje cell and granule cells (Sugiyama et al. 1999; Nakamura et al. 2004), as well as reciprocal expression of PLCβ3 and PLCβ4 in distinct, parasagittaly organized Purkinje cell subsets (Watanabe et al. 1998; Sarna et al. 2006; Nomura et al. 2007). The chemically distinct Purkinje cells form complementary stripes in the cerebellum characterized by low levels of PLCβ3 in PLCβ4-dominant Purkinje cells, and vice versa. The presence of PLCβ1 in Purkinje cell was only recently described in a study detailing the localization of PLCβ1 in rat brain (Montaña et al. 2012). We observed, in both mouse and rat, that the pattern of PLCβ1 immunolabeled Purkinje cells tends to parallel the pattern of PLCβ3, but only in the anterior cerebellum; in the posterior cerebellum the Purkinje cells show a more uniform immunolabeling. Remarkably, the immunolabeling pattern of the flocculonodular lobe and the paraflocculus is unique for each of the three Purkinje cell specific PLCβ isozyme. The diversity of the PLCβ isoforms in the Purkinje cells is intriguing and suggest that different PLCβ isoforms are either involved in distinct signaling pathways or alternatively, they may regulate the same pathways albeit with different potency (Kim et al. 1997; Rhee 2001; Sarna et al. 2006; Nomura et al. 2007; Harden et al. 2009; Adjobo-Hermans et al. 2013).

Type I and type II UBCs exhibit subtype specific distribution

Several studies described diverse subtype specific distribution of UBCs in nodulus and uvula (Diño et al. 1999; Takács et al. 1999; Nunzi et al. 2002; Chung et al. 2009b); some of these studies even noted that UBCs residing in individual folia are not homogenously distributed (Diño et al. 1999; Chung et al. 2009b). The advancing research on UBCs, especially the emergence of two chemically distinct UBC subtypes, however created a need for a comprehensive, subtype-specific analysis encompassing not only the cerebellar vermis but also the cerebellar hemispheres and flocculus/paraflocculus. In this study we constructed several cerebellar maps that show in detail the spatial distribution of type I and type II UBC in two different species, rat and mouse. Analysis of these map confirmed some of the earlier published data (Jaarsma et al. 1998; Diño et al. 1999; Takács et al. 1999; Nunzi et al. 2002; Chung et al. 2009b) but also yielded several new interesting details. Although both UBC subtypes are enriched in the rodent vestibulocerebellum, the localization of type I UBCs is essentially restricted to the flocculonodular lobe, anterior part of ventral uvula and region 1 of the ventral paraflocculus. On the other hand type II UBCs show a widespread localization throughout the cerebellar cortex; they are present in all vermal and hemishperal lobules with exception of vermal lolules V and VIa where type II UBCs are extremely rare. Intriguingly, we observed a peculiar area in posterior uvula, between IXa and IXb (see also Figs. 8, 10, 15), which contained no UBCs in mouse and rare UBCs in rat, even though it is surrounded by areas containing fair numbers of UBC. We suggest, that this UBC-void area, wedged into vestibulocerebellum receives a specific set of intrinsic mossy fibers, which repel UBC and therefore further investigation of this area and the source of its afferents may elucidate environmental clues that determine the spatial distributions of UBC and effect their interactions with local circuits.

It has been reported that the general UBC distribution pattern in the vestibulocerebellum is comparable amongst several different species (Diño et al. 1999; Takács et al. 1999; Mugnaini et al. 2010), although fine details on zonal subtype-specific UBC distribution are missing. Here we report for first time that the two UBC subclasses show similar general and zonal distribution in two species, rat and mouse, with one obvious exception; in mouse the lateral nodular zones contain high UBC densities but not in rat (see also Fig. 7d, 9d). In both species the topographic distribution of UBCs, irrespective of subtypes, is not homogenous, especially along the medio-lateral axis; the highest UBC density patches/zones are near the vermal midline and at the flocculus to paraflocculus transition zone that also includes the region1 of ventral paraflocculus. Not surprisingly, the zonal distribution of type I and type II UBC reveals somehow overlapping but at the same time very diverse subtype specific pattern suggesting that the UBC subtypes differ not only chemically and by their distinct electrophysiological properties (Mugnaini et al. 2010; Kim et al. 2012) but also by the input they receive. A clear example of this subtype-specific pattern would be a narrow midline zone in ventral nodulus where the conspicuously low concentration of $CR^+/PLC\beta1^+$ type I UBCs is paired with very high density of $mGluR1\alpha^+/PLC\beta4^+$ type II UBCs. This region may require a closer attention in the future as it might be supplied with a specific intrinsic mossy fiber set favored by type II UBCs but avoided by type I UBCs.

Recently it was suggested, based on Ebf2 null and scrambler mutant mice studies, that the Purkinje cell phenotypes restrict the topographical distribution of the UBCs (Chung et al. 2009b) and that the CR^+ and $mGluR1\alpha^+$ UBCs are loosely aligned with zebrin II $P1^+$,$P2^+$ and $P3^+$ in dorsal lobule IX. To substantiate these finding we analyzed the topographical distribution of UBCs in relation to PLCβ labeled Purkinje cell stripes and found that both UBC subtypes, $CR^+/PLC\beta1^+$ and $mGluR1\alpha^+/PLC\beta4^+$ alike, are distributed in zonal fashion in high, medium and low density patches/zones which show scarce if any correlation with Purkinje cell stripes. The exception is the region 2 of lobule IXc/d(rat)/IXc(mouse) where high-density patches of both UBC subtypes are loosely associated with $PLC\beta4^-$ Purkinje cell

stripes (equivalent to zebrin II $P1^+$ and $P2^+$), just as described by Chung et al. (2009b). Taken together our observations suggest that albeit the disposition of the UBCs within the cerebellar cortex might be influenced by clustering of early PC cells (Chung et al. 2009b), it is much more likely that the deployment of these interneurons within individual lobules is governed by other factors related to specific afferents, such as primary and secondary vestibular afferents (Jaarsma et al. 1996; Diño et al. 2001). Our data represent a promising first step in expanding the scanty knowledge on afferent fibers that target specific UBC subtypes (Mugnaini et al. 2010) and may define new local microcircuits.

mGluRs and PLCβ activation in UBC

mGluRs and PLCβ isoforms are highly concentrated in the cell's dendritic brush, which comes in intimate contact with mossy fiber terminals in the UBC glomerulus (Mugnaini and Floris 1994; Rossi et al. 1995) and are also highly enriched in the perisynaptic filopodia of the UBCs dendrioles (Jaarsma et al. 1998). It may be suggested that CR play a role in the fast Ca^{2+} signaling following action of voltage-gated Ca^{2+} channels, mGluRs and PLCβ4 may be part of a synaptically activated slower signaling cascade initiated by glutamate molecules that diffuse from synaptic release sites in the intercellular space of the glomerulus, bind to perisynaptic mGluRs, and regulate enzyme activation by second messengers (Ross et al. 2005). This process would lead to dissociation of heterodimeric G proteins and recruitment of PLCβ to the plasma membrane and its activation. Through hydrolyzation of phosphatidylinositol 4,5-biphosphate (PtdInsP2, PIP2) PLCβ activation generates IP3 and 1,2-diacylglycerol (DAG), which may trigger calcium mobilization, vesicle mobilization and activation of various types of effector proteins affecting diverse intracellular and plasma membrane functions and gene expression (Rhee 2001). PIP2 and DAG are also known to directly control different forms of ion channels (Woo et al. 2008; Fukami et al. 2010). Notably, the specific activity of PLCβ4 toward PIP2 is about four times that of PLCβ1 (Lee et al. 1994); however, it is not known whether type I and type II UBC differ in their content of potential Ca^{2+} stores in the form of tubules and vesicles of endoplasmic reticulum harboring calcium permeable channels or in PIP2-DAG signaling activated channels such as TRPC3. In Purkinje cell dendrites, mGluR1α can couple P/Q type $Ca_V2.1$ channels; whether this may also apply to UBCs, however, remains to be ascertained (Kitano et al. 2003; Ferraguti et al. 2008). Membrane phospholipids may also regulate transient receptor potential (TRP) channels, which function as part of large macromolecular assemblies (Wang et al. 2007; Montell 2011). Indeed, mRNAs coding for the members of the canonic TRPC3,6,7 channel group are present in UBCs (Schilling and Oberdick 2009). In view of our sparse knowledge on the UBC proteome, the significance of the differential expression of two different PLCβ isoforms in the type I and type II UBC is a matter of speculation.

The core structure of PLCβ consists of multiple domains - an N-terminal pleckstrin homology (PH) domain, followed by a series of EF-hands motifs, a catalytic TIM barrel incorporating X- and Y-box regions, a C2 domain and a c-terminal tail of ~400 amino acid residues (CT domain) - that can bind multiple ligands (Williams and Katan 1996; Williams 1999; Rebecchi and Pentyala 2000; Rhee 2001; Bunney and Katan 2011). C2 domain is known to bind Ca^{2+} and mediate Ca^{2+} dependent interaction of target proteins with lipid membranes (Rebecchi and Pentyala 2000; Rhee 2001; Lemmon 2008). In PLCβ subfamily, however, the key residues essential for calcium ligation are not conserved (Williams and Katan 1996; Rebecchi and Pentyala 2000) and rather than binding Ca^{2+} this domain interacts with GTP-bound Gαq subunit (Wang et al. 1999). PLCβ isoforms share conserved core elements with the PLC family with exception of CT domain (Williams 1999; Rebecchi and Pentyala 2000; Rhee 2001; Bunney and Katan 2011), which not only shows low, ~30% amino acid identity between the PLCβ isoforms but is also the principal domain changed

upon alternate splicing (Kim et al. 1998; Rhee 2001; Adjobo-Hermans et al. 2013). Changes in CT domain effect the subcellular localization of PLCβ isoforms and the potency of Gq-mediated Ca^{2+} influx inhibition (Adjobo-Hermans et al. 2013), thus different PLCβ isoforms may play role in distinct PLC-mediated signaling transduction. Identification of effector proteins that may relate to either PLCβ1 and/or PLCβ4 in UBCs would therefore represent a worthy enterprise. Indeed, structural and mechanistic studies suggest that PLC activity is stringently regulated by experimentally approachable molecular mechanisms (Bunney and Katan 2011; Adjobo-Hermans et al. 2013), and the UBC might provide a model of a well-defined neuron in which specific mechanisms can be tested. Interestingly, whereas the group 1 metabotropic mGluR1α primarily couple to PLCβ via the Gq/11, the group II metabotropic mGluR2 activates GIRKs through the Gs and Gi/o pathways (Lennon et al. 2010; Bunney and Katan 2011). Notably, GIRK1, GIRK2 and GIRK3 are differentially expressed in type I and type II UBCs (Aguado et al. 2008; Kim et al. 2012).

The present study, thus, provides a new angle to the understanding of diverse signaling pathways in the two main UBC subclasses (Diana et al. 2007; Birnstiel et al. 2009) and complements previous knowledge on the diversity of the chemical phenotypes between the subsets of CR-expressing type I UBCs and mGluR1a-expressing type II UBCs.

Supplementary Material

Refer to Web version on PubMed Central for supplementary material.

Acknowledgments

This work was supported by NIH grant RO1 09904. The authors wish to thank Drs. Joe P. Doyle, Joseph D. Dougherthy and Nataniel Heintz (The Rockefeller University, New York) for breeding pairs of Tg(Grp-EGFP)DV197 mice, Prof. Ryuichi Shigemoto (National Institute for Physiological Sciences, Okazaki, Japan) and Dr. K. Goto (Yamagata University School of Medicine, Japan) mGluR1α and DGKβ antibodies, respectively.

Abbreviations used in the figures

AON	anterior olfactory nucleus
Cer	cerebellum
CN	cerebellar nucleus
Cop	copula
Cx	cortex
DCN	dorsal cochlear nucleus
Fl	flocculus
gcl	granule cell layer
Hip	hippocampus
mb	medullary vellum border
ml	molecular layer
OB	olfactory bulb
PFl	paraflocculus
PM	paramedian lobule
sgl	superficial granular layer

Sim	simple lobule
tz	transition zone
VCN	ventral cochlear nucleus
wm	white matter
roman numerals I-X	cerebellar lobules
I	lingula
VI, VIb, VIc	folia of lobule VI
IX	uvula
IXa, IXb, IXc	folia of uvula
IXc/d	in some rat specimens the last folia of uvula is subdiveded into IXc and IXd by a shallow sulcus.
X	nodulus
X*dors*	dorsal leaflet of nodulus
X*vent*	ventral leaflet of nodulus
r1-r4	regions 1-4; folial subdivision based on UBC densities

References

Adjobo-Hermans MJ, Crosby KC, Putyrski M, Bhageloe A, van Weeren L, Schultz C, Goedhart J, Gadella TW Jr. PLCbeta isoforms differ in their subcellular location and their CT-domain dependent interaction with Galphaq. Cell Signal. 2013; 25:255–263. [PubMed: 23006664]

Aguado C, Colón J, Ciruela F, Schlaudraff F, Cabañero MJ, Perry C, Watanabe M, Liss B, Wickman K, Luján R. Cell type-specific subunit composition of G protein-gated potassium channels in the cerebellum. J Neurochem. 2008; 105:497–511. [PubMed: 18088366]

Berrebi AS, Morgan JI, Mugnaini E. The Purkinje cell class may extend beyond the cerebellum. J Neurocytol. 1990; 19:643–654. [PubMed: 2077109]

Berrebi AS, Mugnaini E. Distribution and targets of the cartwheel cell axon in the dorsal cochlear nucleus of the guinea pig. Anat Embryol (Berl). 1991; 183:427–454. [PubMed: 1862946]

Birnstiel S, Slater NT, McCrimmon DR, Mugnaini E, Hartell NA. Voltage-dependent calcium signaling in rat cerebellar unipolar brush cells. Neuroscience. 2009; 162:702–712. [PubMed: 19409228]

Bunney TD, Katan M. PLC regulation: emerging pictures for molecular mechanisms. Trends Biochem Sci. 2011; 36:88–96. [PubMed: 20870410]

Chung SH, Marzban H, Watanabe M, Hawkes R. Phospholipase Cbeta4 expression identifies a novel subset of unipolar brush cells in the adult mouse cerebellum. Cerebellum. 2009a; 8:267–276. [PubMed: 19165551]

Chung SH, Sillitoe RV, Croci L, Badaloni A, Consalez G, Hawkes R. Purkinje cell phenotype restricts the distribution of unipolar brush cells. Neuroscience. 2009b; 164:1496–1508. [PubMed: 19800947]

Diana MA, Otsu Y, Maton G, Collin T, Chat M, Dieudonné S. T-type and L-type Ca2+ conductances define and encode the bimodal firing pattern of vestibulocerebellar unipolar brush cells. J Neurosci. 2007; 27:3823–3838. [PubMed: 17409247]

Diño MR, Mugnaini E. Distribution and phenotypes of unipolar brush cells in relation to the granule cell system of the rat cochlear nucleus. Neuroscience. 2008; 154:29–50. [PubMed: 18343594]

Diño MR, Perachio AA, Mugnaini E. Cerebellar unipolar brush cells are targets of primary vestibular afferents: an experimental study in the gerbil. Exp Brain Res. 2001; 140:162–170. [PubMed: 11521148]

Diño MR, Schuerger RJ, Liu Y, Slater NT, Mugnaini E. Unipolar brush cell: a potential feedforward excitatory interneuron of the cerebellum. Neuroscience. 2000; 98:625–636. [PubMed: 10891606]

Diño MR, Willard FH, Mugnaini E. Distribution of unipolar brush cells and other calretinin immunoreactive components in the mammalian cerebellar cortex. J Neurocytol. 1999; 28:99–123. [PubMed: 10590511]

Doyle JP, Dougherty JD, Heiman M, Schmidt EF, Stevens TR, Ma G, Bupp S, Shrestha P, Shah RD, Doughty ML, Gong S, Greengard P, Heintz N. Application of a translational profiling approach for the comparative analysis of CNS cell types. Cell. 2008; 135:749–762. [PubMed: 19013282]

Englund C, Kowalczyk T, Daza RA, Dagan A, Lau C, Rose MF, Hevner RF. Unipolar brush cells of the cerebellum are produced in the rhombic lip and migrate through developing white matter. J Neurosci. 2006; 26:9184–9195. [PubMed: 16957075]

Ferraguti F, Crepaldi L, Nicoletti F. Metabotropic glutamate 1 receptor: current concepts and perspectives. Pharmacol Rev. 2008; 60:536–581. [PubMed: 19112153]

Fukami K, Inanobe S, Kanemaru K, Nakamura Y. Phospholipase C is a key enzyme regulating intracellular calcium and modulating the phosphoinositide balance. Prog Lipid Res. 2010; 49:429–437. [PubMed: 20553968]

Fukaya M, Uchigashima M, Nomura S, Hasegawa Y, Kikuchi H, Watanabe M. Predominant expression of phospholipase Cbeta1 in telencephalic principal neurons and cerebellar interneurons, and its close association with related signaling molecules in somatodendritic neuronal elements. Eur J Neurosci. 2008; 28:1744–1759. [PubMed: 18973591]

Harden TK, Hicks SN, Sondek J. Phospholipase C isozymes as effectors of Ras superfamily GTPases. Journal of Lipid Research. 2009; 50(Suppl):S243–248. [PubMed: 19033212]

Harris J, Moreno S, Shaw G, Mugnaini E. Unusual neurofilament composition in cerebellar unipolar brush neurons. J Neurocytol. 1993; 22:1039–1059. [PubMed: 8106879]

Hashimoto K, Miyata M, Watanabe M, Kano M. Roles of phospholipase Cbeta4 in synapse elimination and plasticity in developing and mature cerebellum. Mol Neurobiol. 2001; 23:69–82. [PubMed: 11642544]

Hozumi Y, Fukaya M, Adachi N, Saito N, Otani K, Kondo H, Watanabe M, Goto K. Diacylglycerol kinase beta accumulates on the perisynaptic site of medium spiny neurons in the striatum. European Journal of Neuroscience. 2008; 28:2409–2422. [PubMed: 19087171]

Hozumi Y, Goto K. Diacylglycerol kinase beta in neurons: functional implications at the synapse and in disease. Adv Biol Regul. 2012; 52:315–325. [PubMed: 22781745]

Hozumi Y, Watanabe M, Otani K, Goto K. Diacylglycerol kinase beta promotes dendritic outgrowth and spine maturation in developing hippocampal neurons. BMC Neurosci. 2009; 10:99. [PubMed: 19691842]

Jaarsma D, Diño MR, Cozzari C, Mugnaini E. Cerebellar choline acetyltransferase positive mossy fibres and their granule and unipolar brush cell targets: a model for central cholinergic nicotinic neurotransmission. J Neurocytol. 1996; 25:829–842. [PubMed: 9023728]

Jaarsma D, Diño MR, Ohishi H, Shigemoto R, Mugnaini E. Metabotropic glutamate receptors are associated with non-synaptic appendages of unipolar brush cells in rat cerebellar cortex and cochlear nuclear complex. J Neurocytol. 1998; 27:303–327. [PubMed: 9923978]

Kim D, Jun KS, Lee SB, Kang NG, Min DS, Kim YH, Ryu SH, Suh PG, Shin HS. Phospholipase C isozymes selectively couple to specific neurotransmitter receptors. Nature. 1997; 389:290–293. [PubMed: 9305844]

Kim J-A, Sekerková G, Mugnaini E, Martina M. Electrophysiological, morphological, and topological properties of two histochemically distinct subpopulations of cerebellar unipolar brush cells. Cerebellum. 2012 DOI: 10.1007/s12311-12012-10380-12318.

Kim MJ, Min DS, Ryu SH, Suh PG. A cytosolic, galphaq- and betagamma-insensitive splice variant of phospholipase C-beta4. Journal of Biological Chemistry. 1998; 273:3618–3624. [PubMed: 9452490]

Kitano J, Nishida M, Itsukaichi Y, Minami I, Ogawa M, Hirano T, Mori Y, Nakanishi S. Direct interaction and functional coupling between metabotropic glutamate receptor subtype 1 and voltage-sensitive Cav2.1 Ca2+ channel. J Biol Chem. 2003; 278:25101–25108. [PubMed: 12704197]

Knoflach F, Kemp JA. Metabotropic glutamate group II receptors activate a G protein-coupled inwardly rectifying K+ current in neurones of the rat cerebellum. J Physiol. 1998; 509(Pt 2):347–354. [PubMed: 9575285]

Larsell, O. The comparative anatomy and histology of the cerebellum from monotremes through apes. The University of Minnesota Press; Minneapolis: 1968.

Lee CW, Lee KH, Lee SB, Park D, Rhee SG. Regulation of phospholipase C-beta 4 by ribonucleotides and the alpha subunit of Gq. J Biol Chem. 1994; 269:25335–25338. [PubMed: 7929227]

Lein ES, Hawrylycz MJ, Ao N, Ayres M, Bensinger A, Bernard A, Boe AF, Boguski MS, Brockway KS, Byrnes EJ, Chen L, Chen L, Chen TM, Chin MC, Chong J, Crook BE, Czaplinska A, Dang CN, Datta S, Dee NR, Desaki AL, Desta T, Diep E, Dolbeare TA, Donelan MJ, Dong HW, Dougherty JG, Duncan BJ, Ebbert AJ, Eichele G, Estin LK, Faber C, Facer BA, Fields R, Fischer SR, Fliss TP, Frensley C, Gates SN, Glattfelder KJ, Halverson KR, Hart MR, Hohmann JG, Howell MP, Jeung DP, Johnson RA, Karr PT, Kawal R, Kidney JM, Knapik RH, Kuan CL, Lake JH, Laramee AR, Larsen KD, Lau C, Lemon TA, Liang AJ, Liu Y, Luong LT, Michaels J, Morgan JJ, Morgan RJ, Mortrud MT, Mosqueda NF, Ng LL, Ng R, Orta GJ, Overly CC, Pak TH, Parry SE, Pathak SD, Pearson OC, Puchalski RB, Riley ZL, Rockett HR, Rowland SA, Royall JJ, Ruiz MJ, Sarno NR, Schaffnit K, Shapovalova NV, Sivisay T, Slaughterbeck CR, Smith SC, Smith KA, Smith BI, Sodt AJ, Stewart NN, Stumpf KR, Sunkin SM, Sutram M, Tam A, Teemer CD, Thaller C, Thompson CL, Varnam LR, Visel A, Whitlock RM, Wohnoutka PE, Wolkey CK, Wong VY, Wood M, Yaylaoglu MB, Young RC, Youngstrom BL, Yuan XF, Zhang B, Zwingman TA, Jones AR. Genome-wide atlas of gene expression in the adult mouse brain. Nature. 2007; 445:168–176. [PubMed: 17151600]

Lemmon MA. Membrane recognition by phospholipid-binding domains. Nat Rev Mol Cell Biol. 2008; 9:99–111. [PubMed: 18216767]

Lennon SM, Rivero G, Matharu A, Howson PA, Jane DE, Roberts PJ, Kelly E. Metabotropic glutamate receptor mGlu2 is resistant to homologous agonist-induced desensitization but undergoes protein kinase C-mediated heterologous desensitization. Eur J Pharmacol. 2010; 649:29–37. [PubMed: 20826132]

Min DS, Kim MJ, Jeong HK, Lee YH, Kim H, Shin HS, Ryu SH, Suh PG. Immunological characterization of 130 kDa phospholipase C-beta 4 isozyme in rat cerebellar Purkinje cells. Neurosci Lett. 2000; 292:9–12. [PubMed: 10996437]

Montaña M, García Del Caño G, López de Jesús M, González-Burguera I, Echeazarra L, Barrondo S, Sallés J. Cellular neurochemical characterization and subcellular localization of phospholipase C beta1 in rat brain. Neuroscience. 2012; 222:239–268. [PubMed: 22735577]

Montell C. The history of TRP channels, a commentary and reflection. Pflugers Arch. 2011; 461:499–506. [PubMed: 21287198]

Mugnaini E, Berrebi AS, Dahl AL, Morgan JI. The polypeptide PEP-19 is a marker for Purkinje neurons in cerebellar cortex and cartwheel neurons in the dorsal cochlear nucleus. Arch Ital Biol. 1987; 126:41–67. [PubMed: 3449006]

Mugnaini E, Floris A. The unipolar brush cell: a neglected neuron of the mammalian cerebellar cortex. J Comp Neurol. 1994; 339:174–180. [PubMed: 8300904]

Mugnaini E, Floris A, Wright-Goss M. Extraordinary synapses of the unipolar brush cell: an electron microscopic study in the rat cerebellum. Synapse. 1994; 16:284–311. [PubMed: 8059339]

Mugnaini E, Sekerkova G, Martina M. The unipolar brush cell: a remarkable neuron finally receiving deserved attention. Brain Res Rev. 2010; 66:220–245. [PubMed: 20937306]

Nakamura M, Sato K, Fukaya M, Araishi K, Aiba A, Kano M, Watanabe M. Signaling complex formation of phospholipase Cbeta4 with metabotropic glutamate receptor type 1alpha and 1,4,5-trisphosphate receptor at the perisynapse and endoplasmic reticulum in the mouse brain. Eur J Neurosci. 2004; 20:2929–2944. [PubMed: 15579147]

Neki A, Ohishi H, Kaneko T, Shigemoto R, Nakanishi S, Mizuno N. Pre- and postsynaptic localization of a metabotropic glutamate receptor, mGluR2, in the rat brain: an immunohistochemical study with a monoclonal antibody. Neurosci Lett. 1996; 202:197–200. [PubMed: 8848265]

Nomura S, Fukaya M, Tsujioka T, Wu D, Watanabe M. Phospholipase Cbeta3 is distributed in both somatodendritic and axonal compartments and localized around perisynapse and smooth

endoplasmic reticulum in mouse Purkinje cell subsets. Eur J Neurosci. 2007; 25:659–672. [PubMed: 17298601]

Nunzi MG, Birnstiel S, Bhattacharyya BJ, Slater NT, Mugnaini E. Unipolar brush cells form a glutamatergic projection system within the mouse cerebellar cortex. J Comp Neurol. 2001; 434:329–341. [PubMed: 11331532]

Nunzi MG, Shigemoto R, Mugnaini E. Differential expression of calretinin and metabotropic glutamate receptor mGluR1alpha defines subsets of unipolar brush cells in mouse cerebellum. J Comp Neurol. 2002; 451:189–199. [PubMed: 12209836]

Ohishi H, Shigemoto R, Nakanishi S, Mizuno N. Distribution of the messenger RNA for a metabotropic glutamate receptor, mGluR2, in the central nervous system of the rat. Neuroscience. 1993a; 53:1009–1018. [PubMed: 8389425]

Ohishi H, Shigemoto R, Nakanishi S, Mizuno N. Distribution of the mRNA for a metabotropic glutamate receptor (mGluR3) in the rat brain: an in situ hybridization study. J Comp Neurol. 1993b; 335:252–266. [PubMed: 8227517]

Pin JP, Duvoisin R. The metabotropic glutamate receptors: structure and functions. Neuropharmacology. 1995; 34:1–26. [PubMed: 7623957]

Rebecchi MJ, Pentyala SN. Structure, function, and control of phosphoinositide-specific phospholipase C. Physiological Reviews. 2000; 80:1291–1335. [PubMed: 11015615]

Rhee SG. Regulation of phosphoinositide-specific phospholipase C. Annu Rev Biochem. 2001; 70:281–312. [PubMed: 11395409]

Ross WN, Nakamura T, Watanabe S, Larkum M, Lasser-Ross N. Synaptically activated ca2+ release from internal stores in CNS neurons. Cell Mol Neurobiol. 2005; 25:283–295. [PubMed: 16047542]

Rossi DJ, Alford S, Mugnaini E, Slater NT. Properties of transmission at a giant glutamatergic synapse in cerebellum: the mossy fiber-unipolar brush cell synapse. J Neurophysiol. 1995; 74:24–42. [PubMed: 7472327]

Rousseau CV, Dugue GP, Dumoulin A, Mugnaini E, Dieudonne S, Diana MA. Mixed inhibitory synaptic balance correlates with glutamatergic synaptic phenotype in cerebellar unipolar brush cells. The Journal of Neuroscience. 2012; 32:4632–4644. [PubMed: 22457509]

Roustan P, Abitbol M, Menini C, Ribeaudeau F, Gerard M, Vekemans M, Mallet J, Dufier JL. The rat phospholipase C beta 4 gene is expressed at high abundance in cerebellar Purkinje cells. Neuroreport. 1995; 6:1837–1841. [PubMed: 8547579]

Russo MJ, Yau HJ, Nunzi MG, Mugnaini E, Martina M. Dynamic metabotropic control of intrinsic firing in cerebellar unipolar brush cells. J Neurophysiol. 2008; 100:3351–3360. [PubMed: 18945818]

Sarna JR, Marzban H, Watanabe M, Hawkes R. Complementary stripes of phospholipase Cbeta3 and Cbeta4 expression by Purkinje cell subsets in the mouse cerebellum. J Comp Neurol. 2006; 496:303–313. [PubMed: 16566000]

Schilling K, Oberdick J. The treasury of the commons: making use of public gene expression resources to better characterize the molecular diversity of inhibitory interneurons in the cerebellar cortex. Cerebellum. 2009; 8:477–489. [PubMed: 19554387]

Sekerková G, Ilijic E, Mugnaini E. Time of origin of unipolar brush cells in the rat cerebellum as observed by prenatal bromodeoxyuridine labeling. Neuroscience. 2004; 127:845–858. [PubMed: 15312897]

Shigemoto R, Kinoshita A, Wada E, Nomura S, Ohishi H, Takada M, Flor PJ, Neki A, Abe T, Nakanishi S, Mizuno N. Differential presynaptic localization of metabotropic glutamate receptor subtypes in the rat hippocampus. J Neurosci. 1997; 17:7503–7522. [PubMed: 9295396]

Sugiyama T, Hirono M, Suzuki K, Nakamura Y, Aiba A, Nakamura K, Nakao K, Katsuki M, Yoshioka T. Localization of phospholipase Cbeta isozymes in the mouse cerebellum. Biochem Biophys Res Commun. 1999; 265:473–478. [PubMed: 10558892]

Takács J, Markova L, Borostyánkői Z, Görcs TJ, Hámori J. Metabotrop glutamate receptor type 1a expressing unipolar brush cells in the cerebellar cortex of different species: a comparative quantitative study. J Neurosci Res. 1999; 55:733–748. [PubMed: 10220114]

Tanaka J, Nakagawa S, Kushiya E, Yamasaki M, Fukaya M, Iwanaga T, Simon MI, Sakimura K, Kano M, Watanabe M. Gq protein alpha subunits Galphaq and Galpha11 are localized at postsynaptic extra-junctional membrane of cerebellar Purkinje cells and hippocampal pyramidal cells. European Journal of Neuroscience. 2000; 12:781–792. [PubMed: 10762307]

Tanaka O, Kondo H. Localization of mRNAs for three novel members (beta 3, beta 4 and gamma 2) of phospholipase C family in mature rat brain. Neurosci Lett. 1994; 182:17–20. [PubMed: 7891878]

Tateyama M, Kubo Y. The intra-molecular activation mechanisms of the dimeric metabotropic glutamate receptor 1 differ depending on the type of G proteins. Neuropharmacology. 2011; 61:832–841. [PubMed: 21672544]

Vitale M, Rezzani R, Gobbi G, Ponti C, Matteucci A, Cacchioli A, Ruggeri A Jr. Cocco L. Phospholipase-C beta1 is predominantely expressed in the granular layer of rat cerebellar cortex. Int J Mol Med. 2004; 14:161–164. [PubMed: 15254758]

Wang M, Bianchi R, Chuang SC, Zhao W, Wong RK. Group I metabotropic glutamate receptor-dependent TRPC channel trafficking in hippocampal neurons. J Neurochem. 2007; 101:411–421. [PubMed: 17402970]

Wang T, Pentyala S, Elliott JT, Dowal L, Gupta E, Rebecchi MJ, Scarlata S. Selective interaction of the C2 domains of phospholipase C-beta1 and -beta2 with activated Galphaq subunits: an alternative function for C2-signaling modules. Proc Natl Acad Sci U S A. 1999; 96:7843–7846. [PubMed: 10393909]

Watanabe M, Nakamura M, Sato K, Kano M, Simon MI, Inoue Y. Patterns of expression for the mRNA corresponding to the four isoforms of phospholipase Cbeta in mouse brain. Eur J Neurosci. 1998; 10:2016–2025. [PubMed: 9753089]

Williams RL. Mammalian phosphoinositide-specific phospholipase C. Biochim Biophys Acta. 1999; 1441:255–267. [PubMed: 10570253]

Williams RL, Katan M. Structural views of phosphoinositide-specific phospholipase C: signalling the way ahead. Structure. 1996; 4:1387–1394. [PubMed: 8994965]

Woo DH, Jung SJ, Zhu MH, Park CK, Kim YH, Oh SB, Lee CJ. Direct activation of transient receptor potential vanilloid 1(TRPV1) by diacylglycerol (DAG). Mol Pain. 2008; 4:42. [PubMed: 18826653]

Yakunin AF, Hallenbeck PC. A luminol/iodophenol chemiluminescent detection system or western immunoblots. Anal Biochem. 1998; 258:146–149. [PubMed: 9527863]

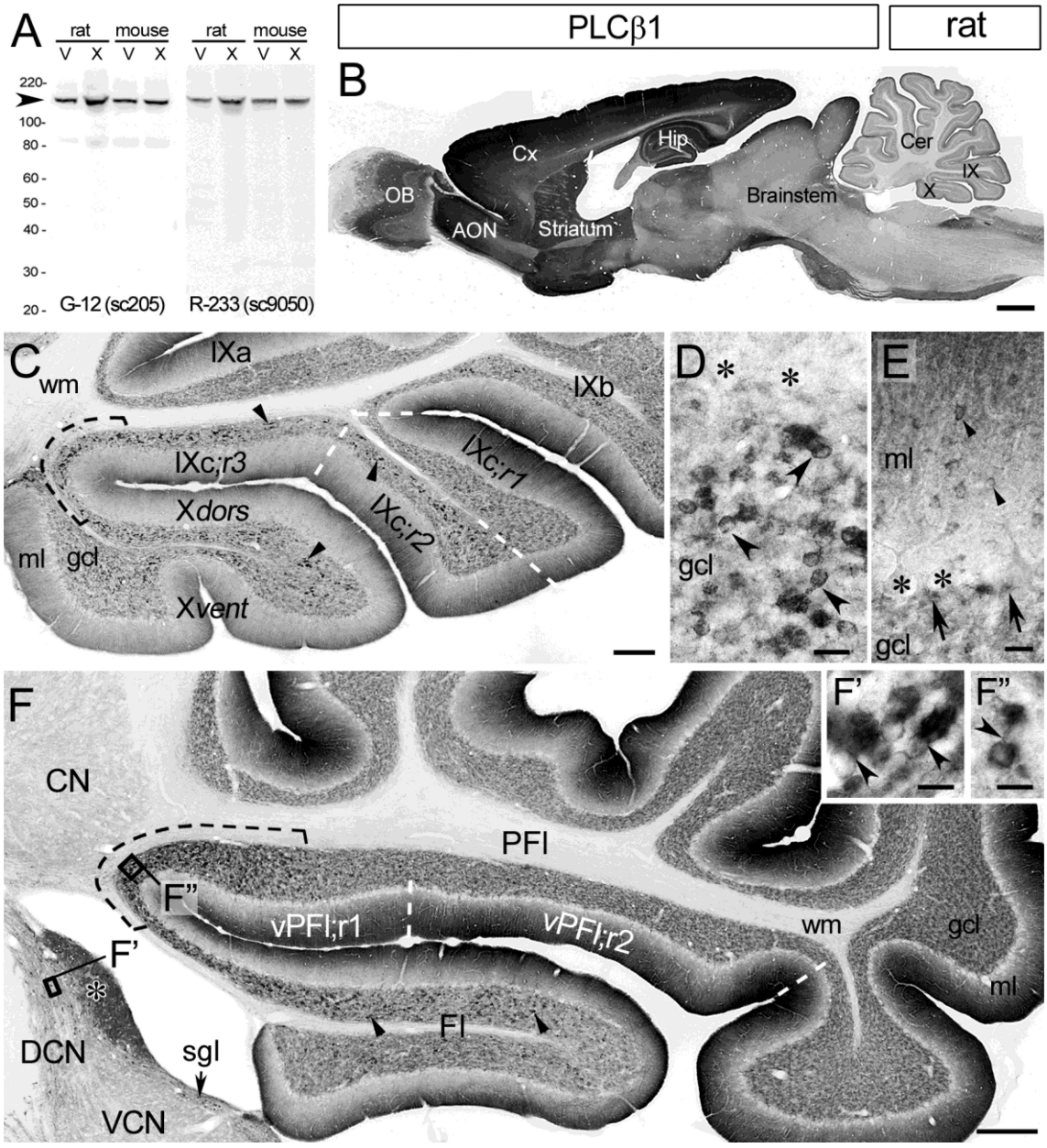

Fig. 1.

PLCβ1-immunoreactivity in rat and mouse cerebellum. **a** Western blots of lobules V and X show PLCβ1 antisera G-12 (sc205) and R-233 (sc9050) recognize a single band at ~145-150 KDa (arrowhead) matching the molecular weight of PLCβ1. **b–f** DAB immunoreacted cryosections of rat cerebella labeled with G-12 (sc205). **b** Median parasagittal section shows intense PLCβ1 immunoreactivity in olfactory bulb, AON, cortex, hippocampus, and striatum, while brainstem and cerebellum are moderately stained. **c** Enlarged image of nodulus and uvula. Note a graded, distal to proximal immunostaining in ml and an overall moderate-to-low immunostaining in gcl. UBCs (arrowheads) are distinctly stained in nodulus and IXc;r2&r3, particularly in the tz IX to X (black dash line). Few PLCβ1^{+} UBC are present in the rest of the uvula, including IXc;r1. Regions 1-3 of IXc are divided by white dashed line. **d** Detail from nodulus shows high density of PLCβ1^{+} UBCs (arrowheads). Purkinje cell bodies (asterisks) are unstained. **e** Detail from lobule V shows

moderate staining of basket/stellate cell somata (arrowheads) and basket cell pinceaux (arrows) beneath the Purkinje cell somata (asterisks). The Purkinje dendritic arbor shows increasing proximo-distal gradient of labeling. **f** Fl, PFl, lateral CN and adjacent brain stem in coronal section. High densities of PLCβ1$^+$ UBC (arrowheads) are detected in Fl and vPFl;r1, especially in the transition zone between the two structures (black dashed line). The CN shows diffuse, faint immunostaining. In the cochlear nuclear complex, PLCβ1$^+$ UBCs occur in DCN and in sgl (arrow), but not in the VCN. In DCN the molecular layer (asterisks) shows distinct immunolabeling. **Insets f' and f"** Enlargements of boxed areas from panel **f** show PLCβ1$^+$ UBCs (arrowheads). The wm is unlabeled (**c, f**). *Scale bars* **b** 1mm, **c, f** 200 μm, **d, e** 20 μm, insets **f'** and **f"** 10 μm

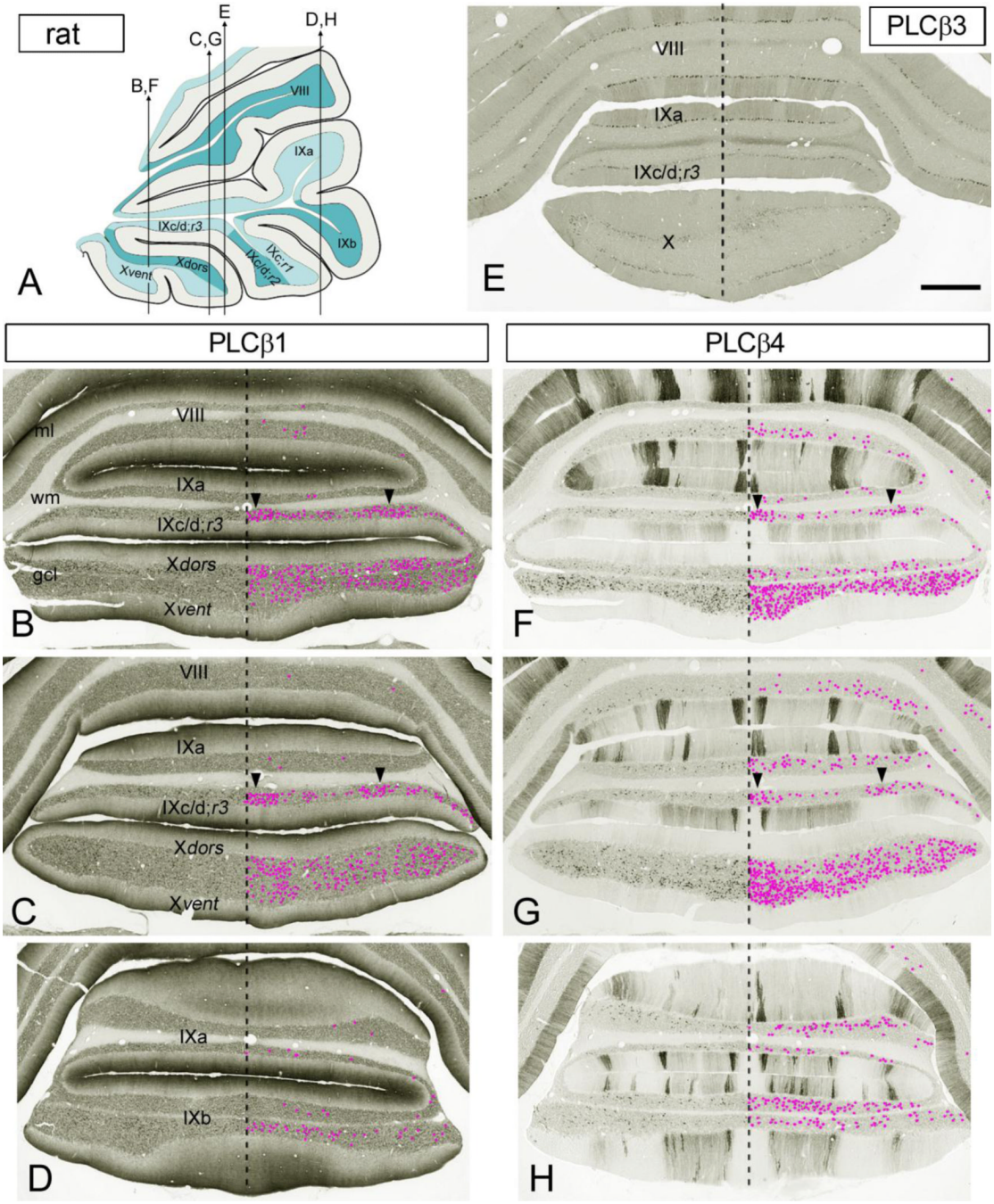

Fig. 2.

Cryosections of the rat posterior cerebellum immunostained with antibodies to different PLCβ isozymes. **a** Schematic parasagittal representation showing the approximate planes of the coronal cerebellar sections in **b-h**. Note, sections shown in panels **b, c,** and **d** are adjacent to the sections shown in panels **f, g,** and **h**, respectively. Dashed line marks the cortical midline. PLCβ1^{+} UBCs (**b-d**) and PLCβ4^{+} UBCs (**f-h**) in the gcl are marked by magenta dots. **b-d** PLCβ1 (G-12; sc205) immunostaining of the Purkinje dendritic arbor in the ml shows an increasing proximo-distal gradient. The nodulus and IXc/d;r3 contain the highest densities of PLCβ1^{+} UBCs (**b, c**), whereas the other lobules contain few PLCβ1^{+}

UBCs (**b-d**). The nodulus shows a nearly even distribution of PLCβ1^{+} UBCs, albeit their density appears somewhat higher near the midline. Arrowheads in IXc/d;r3 (**b, c**) indicate high density PLCβ1^{+} UBC bands; the midline band is particularly rich in PLCβ1^{+} UBCs. **e** The guinea pig PLCβ3 antibody from Frontier Institute labels the Purkinje cell somata, but the ml shows only faint immunostaining; UBCs are unstained. **f-h** PLCβ4^{+} immunolabeling reveals on/off bands of stained Purkinje dendrites in the ml, except in the nodulus, in which the Purkinje cells are either PLCβ4^{-} or only faintly immunolabeled (**f, g**). PLCβ4^{+} UBCs are present at high concentrations in nodulus, IXb, and IXc/d;r3 (**f-g**). The Xvent (**f, g**) contains the highest density of PLCβ4^{+} UBCs, especially in a region close to the midline. At anterior levels (**f**) the density of PLCβ4^{+} UBCs decreases in the Xdors (**f**). The distribution of PLCβ4^{+} UBCs extends to other lobules (**f-h**). Notably, the distribution of PLCβ4^{+} UBC is not in clear register with the PC on/off bands, with exception of IXc/d;r3 where high density UBC bands (arrowheads) are situated beneath PLCβ4^{-} Purkinje cell bands. *Scale bars* **e** 0.5 mm (applies to **b-h**)

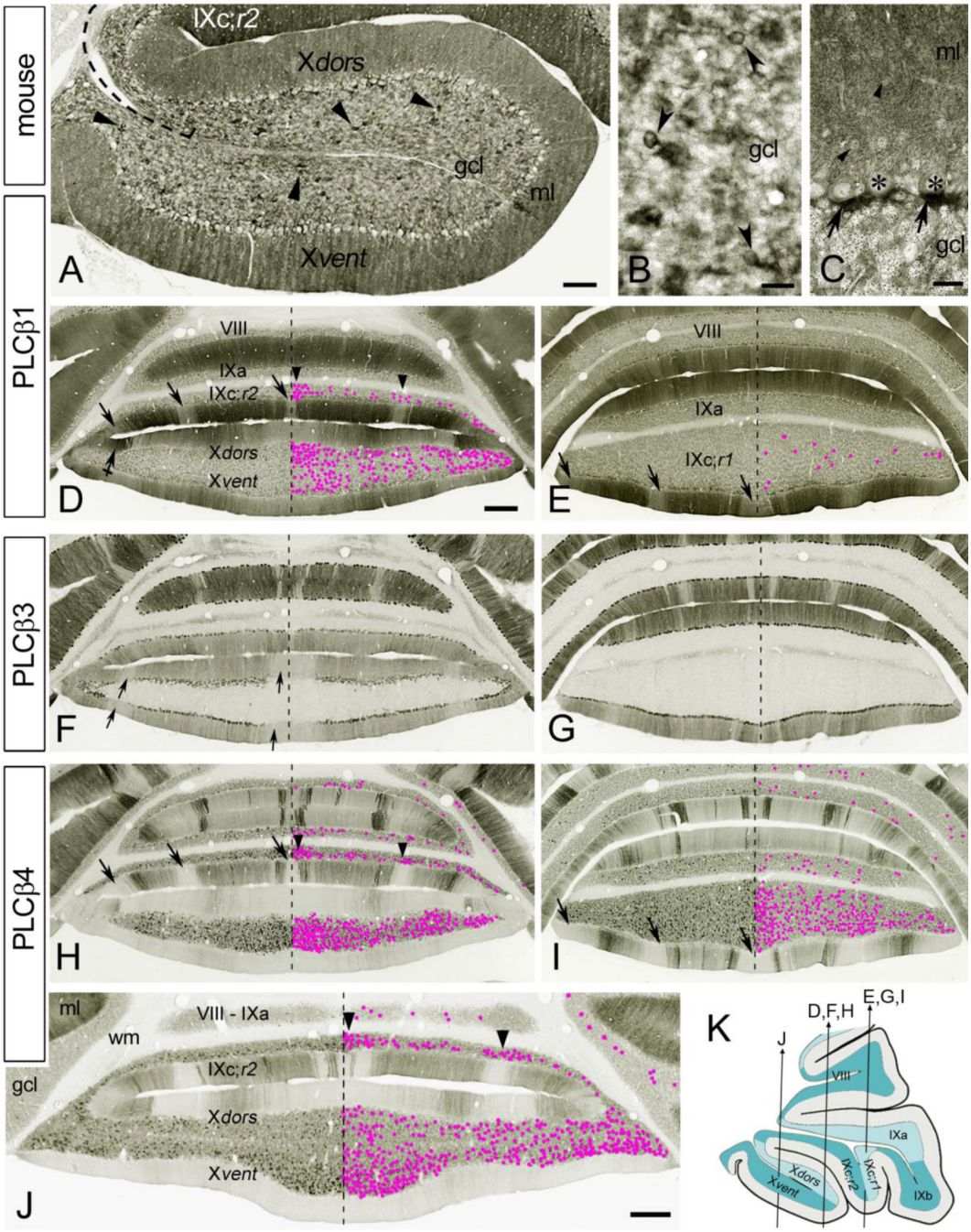

Fig. 3.

Cryosections of the mouse cerebellum immunostained with antibodies to PLCβ1 R-233 (sc9005) (**a-e**), PLCβ3 (Frontier Institute) (**f, g**), and PLCβ4 (**h-j**). **a** Parasagittal paraffin section of nodulus shows moderate PLCβ1 staining throughout the gcl. The somata and brushes of UBCs (arrowheads) are noticeably PLCβ1^{+}. Note the moderately immunopositive Purkinje cell bodies with unstained nuclei and the homogeneous immunolabeling of the ml. Dashed line delineate the tz between IX and X. **b** Representative PLCβ1^{+} UBCs (arrowheads) from the nodulus; cryosection. **c** Detail from lobule V shows moderately stained cell bodies of basket/stellate cells (arrowheads) and intensely PLCβ1^{+} pinceaux

(arrows) below the Purkinje cell somata (asterisks); paraffin section. **d, e** Purkinje arbors in the ml display moderate to intense PLCβ1 immunostaining. Few lighter stained bands (arrows) are noticeable, especially in IXc;r1&r2. The nodulus and IXc;r2 contain the highest densities of PLCβ1^{+} UBCs (**d**), especially the midline portion of IXc;r2. Few PLCβ1^{+} UBCs are present in IXc;r1 (**e**), while PLCβ1^{+} UBCs are absent in other lobules included in sections (**d, e**). Bands with high densities of PLCβ1^{+} UBCs (arrowheads) are present in IXc;r2. Crossed arrow point to intensely labeled lateral stripe in Xdors. **f, g** PLCβ3-immunostaining shows on/off Purkinje cell band in the ml. The PLCβ3 and PLCβ4 show reciprocal immunostaining in the Purkinje cells bands, with exception in nodulus and IXc;r2. UBCs are PLCβ3^{-}. In nodulus three PLCβ3^{-} Purkinje cell stripes are present, in both Xdors and Xvent (arrows); one wide stripe at midline and 2 lateral stripes (one on each side). **h-j** The ml shows on/off bands of PLCβ4–immunoreactivity in Purkinje arbors. In the nodulus many Purkinje cells are PLCβ4^{-}, especially in the Xvent (**h, j**). PLCβ4^{+} UBCs are present at high concentration in nodulus and IXc;r1&r2 (**h-j**), and especially in median portions of the Xvent and IXc;r2 (**h, j**). PLCβ4^{+} UBCs are also present in other lobules (**h-j**). The distribution of PLCβ4^{+} UBCs does not seem in register with Purkinje cell on/off bands, with the exception of IXc;r2 (**h, j**), in which high density UBC bands are situated approximately beneath PLCβ4^{-} Purkinje cell bands (arrowheads). In IXc;r1&r2 the PLCβ4^{-} bands (arrows) are situated at the same position as are the moderately stained PLCβ1^{+} bands in the adjacent sections (arrows in **d, e**). **k** Schematic drawing showing the approximate planes of the coronal cerebellar sections in **d-j**. Panels **e, f**, and **h** show adjacent sections, as do panels **e, g**, and **i**. Dashed line in panels **d-j** indicates the cortical midline. PLCβ1^{+} UBCs (**d, e**) and PLCβ4^{+} UBCs (**h-j**) in the gcl are marked by magenta dots. *Scale bars* **a** 200 μm,**b, c** 20 μm, **d, j** 0.5 mm (**d** applies to **d-i**)

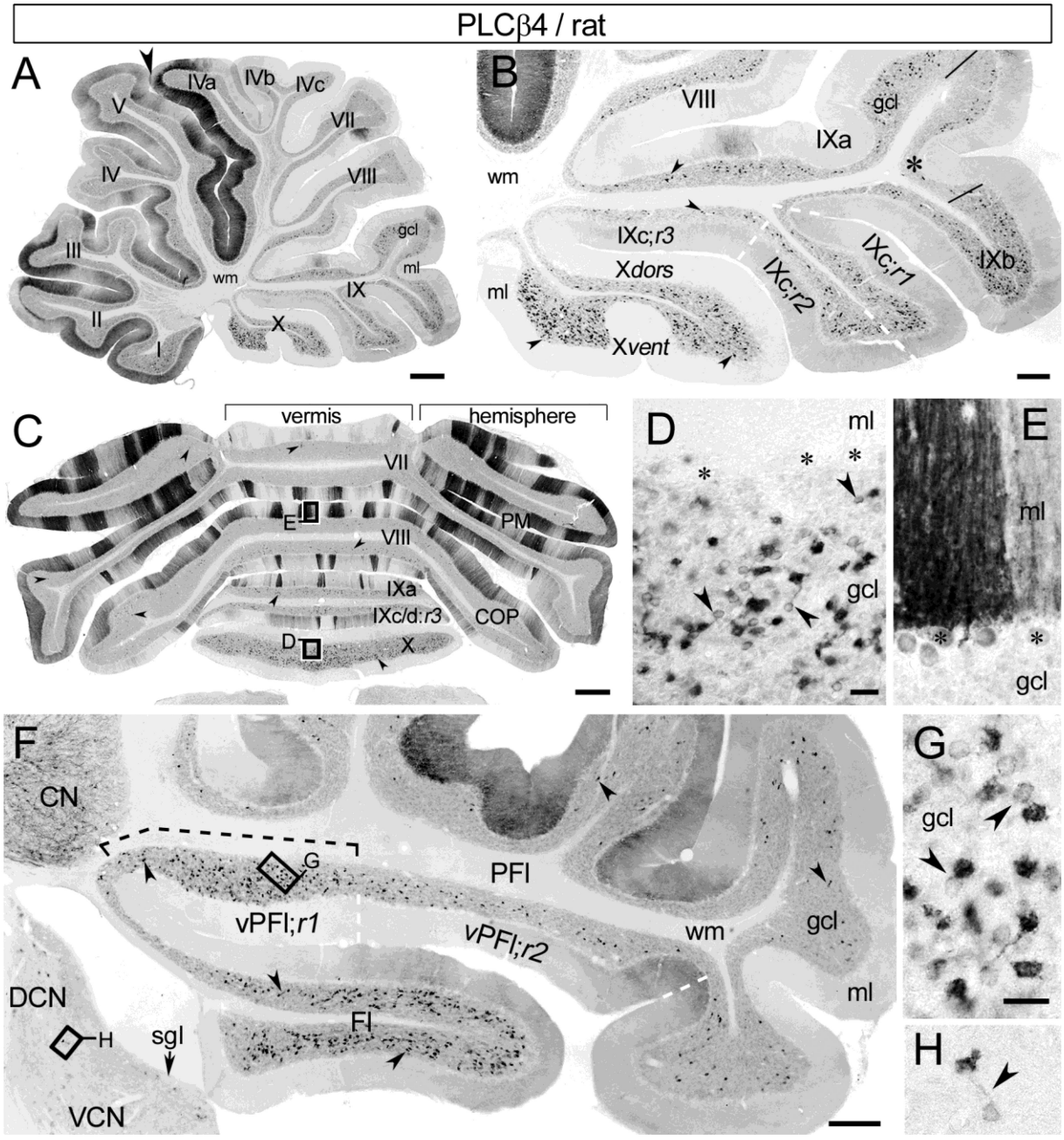

Fig. 4.

PLCβ4-immunoreactivity in rat cerebellum using DAB chromogen. **a** Distributions of PLCβ4-immunostained Purkinje cells and UBCs in a sagittal midvermal section. At this particular level the Purkinje cells are most intensely stained in anterior lobules I-V and around the primary fissure (arrowhead), while many of them they are unstained in posterior lobules VIb, VIc and VII-X. The UBC-rich nodulus, uvula, and lingula show distinct PLCβ4 immunolabeling in the gcl. **b** PLCβ4^{+} UBC (arrowheads) are widespread throughout the nodulus and uvula and also occur in VIII. Asterisk marks an area (between black solid lines) with low density of PLCβ4^{+} UBCs at the IXa-IXb transition. The Xvent contains the highest density of PLCβ4^{+} UBCs; the nodular ml is immunonegative. Region 1-3 of IXc are divided by white dashed line. **c** Coronal section of the posterior cerebellum illustrates PLCβ4

immunostaining in parasagittallly oriented Purkinje cell stripes, and shows the distribution of PLCβ4^{+} UBCs (arrowheads). The nodulus displays the highest density of PLCβ4^{+} UBCs, but other vermal and hemispheral lobules also contain several PLCβ4^{+} UBCs. **d** Enlargement of boxed area from panel **c** shows a densely PLCβ4^{+} UBC population (arrowheads) in nodulus. Asterisks indicate PLCβ4^{-} Purkinje cell bodies. **e** Enlargement of boxed area from panel **c** shows adjacent, intensely and moderately immunopositive Purkinje cell dendrites, arising from their less intensely labeled parent cell bodies (asterisks). **f** Fl, PFl, lateral CN and adjacent brain stem from a coronal section. PLCβ4^{+} UBC (arrowheads) are present in both Fl and PFl, with a notable high density in vPFl;r1 (black dashed line). In CN small neurons are distinctly immunolabeled, while the neuropil shows moderate staining. PLCβ4^{+} UBC are also present in the DCN (**h**) and sgl (arrow), but not in the VCN. **g, h** Enlargement of boxed areas in panel **f** show PLCβ4^{+} UBCs (arrowheads) in PFl (**g**) and in DCN (**h**). The cerebellar wm is unstained (**a, b, f**). *Scale bars* **a, c** 0.5 mm, **b, f** 200 μm, **d, e**, 25 μm, **g, h** 20 μm

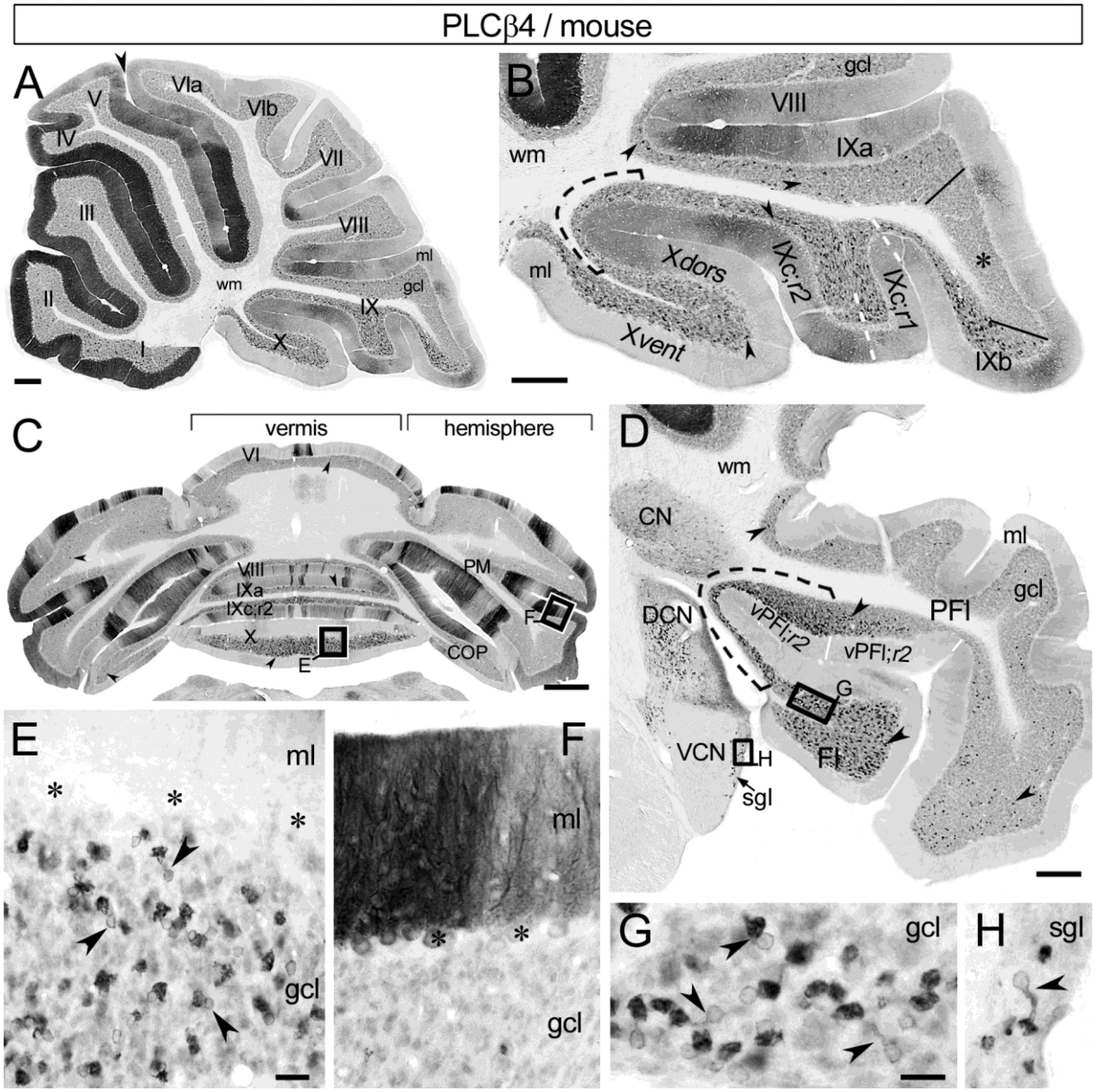

Fig. 5.

PLCβ4-immunoreactivity in mouse cerebellum visualized by DAB chromogen. **a** Sagittal midvermal section illustrates the distributions of PLCβ4-immunostained Purkinje cells and UBCs. At this particular vermal level the Purkinje cells in anterior lobules I-V and around the primary fissure (arrowhead) show the most immunolabeling, while they are either moderately labeled or unstained in the posterior lobules VIb and VII-X. The UBC-rich nodulus, uvula and lingula show distinct PLCβ4 immunoreactivity in the gcl. **b** Enlargement of the caudal cerebellum illustrates the distribution of PLCβ4^{+} UBC (arrowheads) in the gcl. Nodulus, IXc;r1&2 (delineated by white dashed line), and IXb contain the highest densities of PLCβ4^{+} UBCs. Tz IX to X is indicated by black dashed line. Few PLCβ4^{+} UBCs are present in IXa and VIII. Asterisk marks a distinct field of uvula (between IXa and IXb, delineated with solid lines) that is devoid of UBCs. Most of the Purkinje cells in nodulus are PLCβ4^{-}. **c** Coronal section of the posterior cerebellum displays the parasagittal stripes of the PLCβ4^{+} Purkinje cells and the distribution of PLCβ4^{+} UBC (arrowheads). The nodulus and

uvula show the highest density of PLCβ4^{+} UBCs, additionally, scattered PLCβ4^{+} UBCs are distributed in other vermal and hemispheral lobules. **d** Fl, PFl, lateral CN, and adjacent brain stem in coronal section. High densities of PLCβ4^{+} UBCs (arrowheads) occur in Fl and vPFl;r1&2, especially at the transition zone between the two structures (black dashed line). In CN small neurons are distinctly immunolabeled, while the neuropil shows moderate staining. Within the cochlear nuclear complex, PLCβ4^{+} UBCs occur in the DCN and the sgl (arrow), but not in the VCN. **e** Enlarged boxed area from panel **c** shows a dense PLCβ4^{+} UBC population (arrowheads) in nodulus. Asterisks mark PLCβ4^{-} Purkinje cell bodies. **f** Enlarged boxed area from panel **c** shows adjacent, intensely and moderately immunolabeled Purkinje cell dendrites. Asterisks indicate Purkinje cell bodies. **g, h** Enlarged boxed areas from panel **d** show PLCβ4^{+} UBCs (arrowheads) in Fl (**g**) and in sgl (**h**). The cerebellar wm is unstained (**a, b, d**). *Scale bars* **a-d** 200 μm, **e, f** 25 μm, **g, h** 20 μm

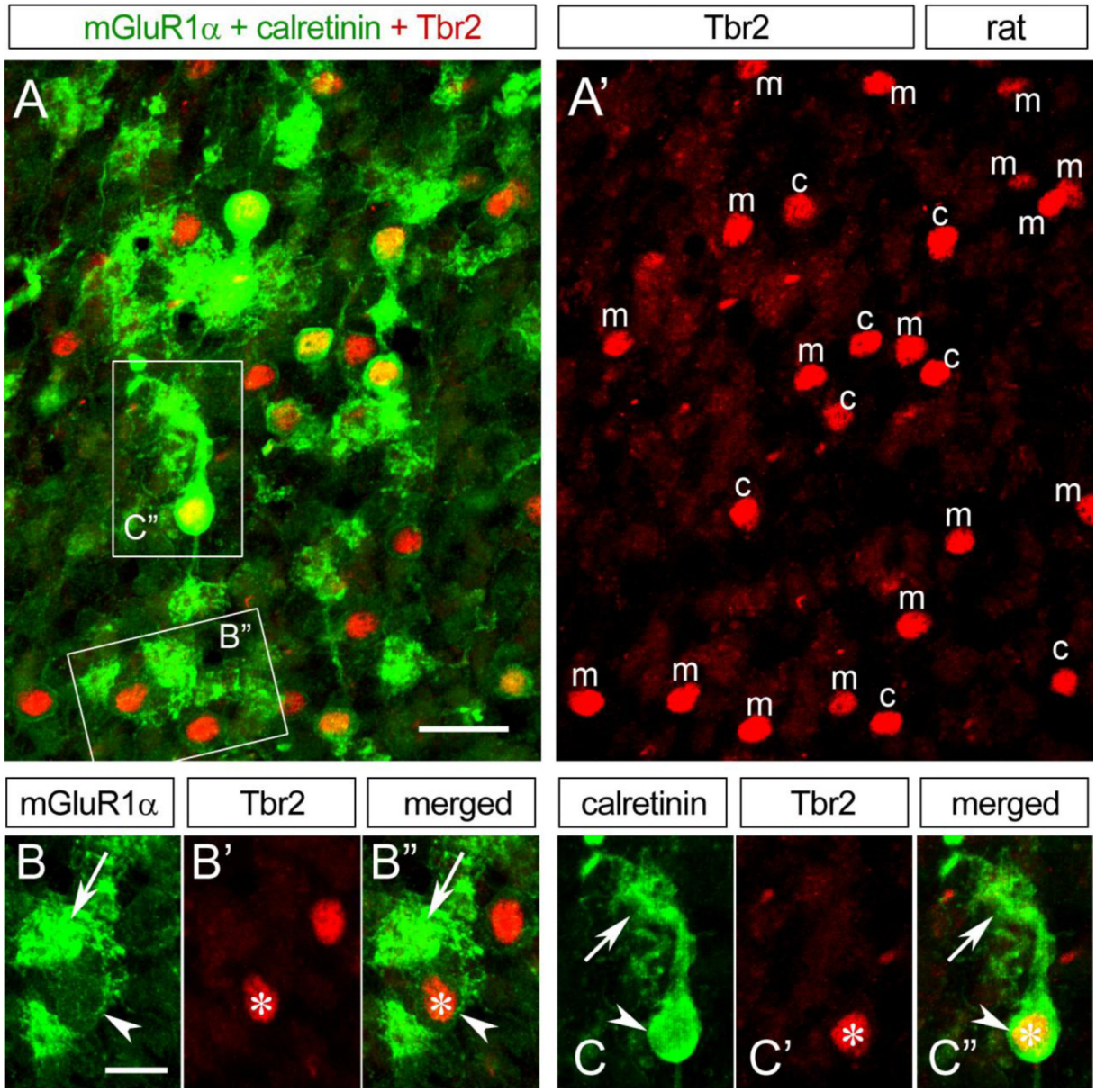

Fig. 6.

Two-color confocal immunofluorescence images of the rat nodulus; cryosections were labeled with cocktails of antibodies to Tbr2, CR and mGluR1α. The cocktail compositions were designed to ascertain whether the sum of the CR^+ and $mGluR1\alpha^+$ UBC subclasses accounts for the entire UBC population. Tbr2 is a marker for all UBC nuclei; CR and mGluR1α are UBC subclass-specific. **a** The section was immunoreacted with a mixture of all three primary antibodies. The Tbr2 binding sites were revealed with Alexa 594-labeled secondary antibody (red), while binding sites of both CR and mGluR1α were revealed with Alexa 488-labeled secondary antibody (green). All UBCs, whether CR^+ or $mGluR1\alpha^+$ possess $Tbr2^+$ nuclei. **a'** Distribution of the CR^+ (c) and $mGluR1\alpha^+$ (m) UBCs associated with Tbr2-labeled nuclei. **b, b', b"** Enlarged boxed area from panel **a** illustrates a typical $mGluR1\alpha^+/Tbr2^+$ UBC; intense staining in the brush (arrow) and subtle immunopositivity in soma (arrowhead). **c, c', c''** Enlarged boxed area from panel **a** illustrates a typical CR^+/

Tbr2$^+$ UBC; intense staining in the brush (arrow) and cell body (arrowhead). Asterisk indicates Tbr2$^+$ UBC nuclei (**b', b", c', c"**). *Scale bars* **a, a'** 20 μm, **b-b''** and **c-c''**10 μm

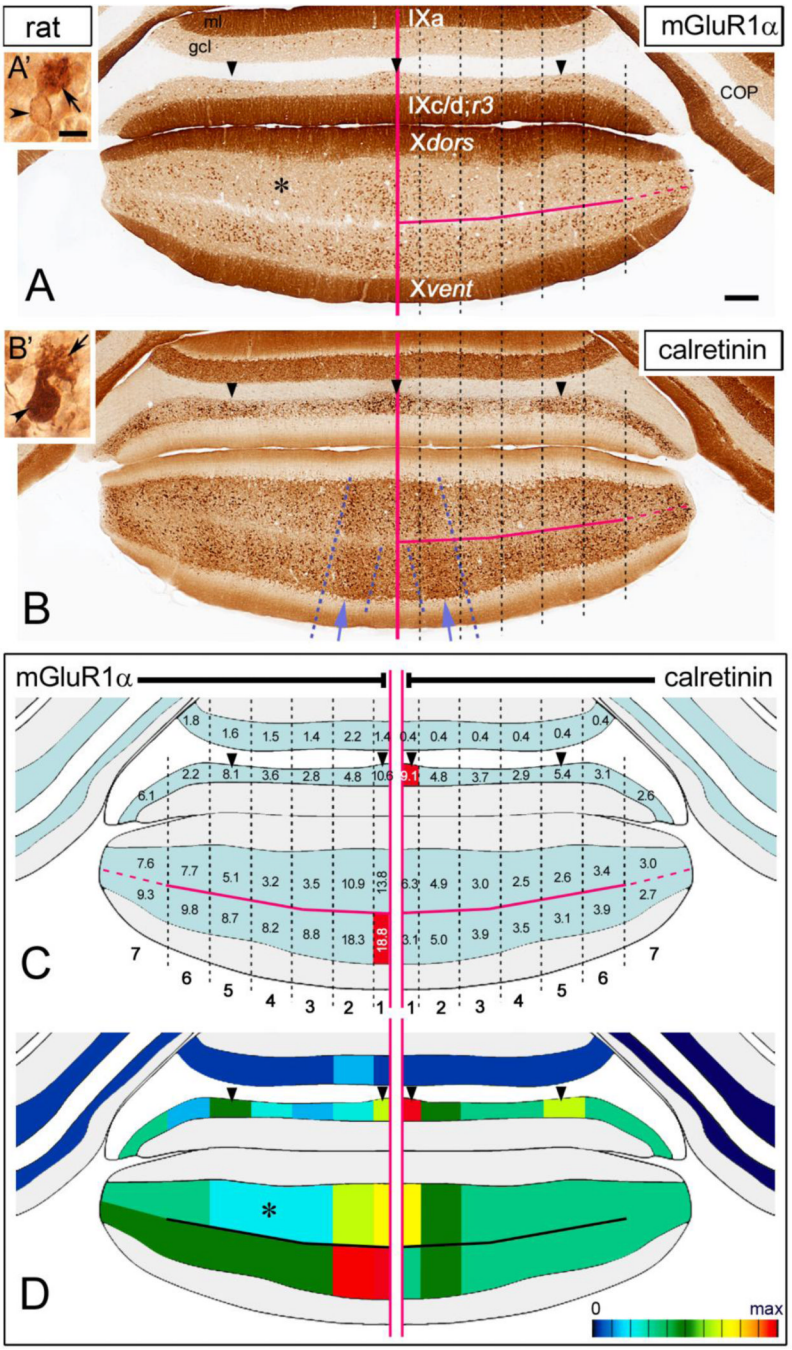

Fig. 7.

Distribution of mGluR1α$^+$ and CR$^+$ UBCs in rat nodulus and uvula as seen in coronal sections. The midline of each section is indicated with horizontal, magenta colored line. Mid-to-lateral zones 1-7 are marked with black dashed lines. Arrowheads indicate UBC rich bands in IXc/d;r3. **a** Typical mGluR1α immunolabeling; intense immunolabeling of Purkinje cell dendrites in ml and distinct immunopositivity in gcl UBCs, especially in nodulus and IXc/d;r3. The highest density of mGluR1α$^+$ UBCs is present around midline. Xdors contain an area encompassing zone 3-5 with low UBC density (asterisk). **Inset a'** shows a representative mGluR1α$^+$ UBC; intense staining in the brush (arrow) and subtle

immunopositivity in soma (arrowhead). **b** Typical CR immunolabeling in UBCs and granule cells. The granule cells somata in gcl and their axons (parallel fibers) in the ml show intense immunopositivity in all cerebellar lobules (IXa, COP shown) except the nodulus and IXc;r2. These later structures contain a dense CR^+ UBC population and CR^+ mossy fibers. Purple dash line delineate an area (purple arrows) with especially dense population of CR labeled UBCs and mossy fibers. **Inset b'** shows a representative CR^+ UBC; intense staining in the brush (arrow) and cell body (arrowhead). **c** Schematic illustration of the mGluR1α^+ (left side) and CR^+ (right side) UBC distributions in mid-to-later zones. Numbers indicate the density of UBCs ($N/0.01mm^2$; for standard deviations see Supplementary Table 1). Midline zones 1 of Xvent and IXc/d;r3 contain the highest densities (red colored zones) of CR^+ UBCs and mGluR1α^+ UBCs, respectively. **d** A gradient map illustrates the distribution of CR^+ UBCs(right side) and mGluR1α^+ UBC (left side). Asterisk marks a sparse mGluR1α^+ UBC region in Xdors. Red color is associated with the highest cell density (max) of either CR^+ UBCs or mGluR1α^+ UBCs. The deep blue colored area contain hardly any UBCs. *Scale bars* **a** 200 μm (applies to **a-d**), **inset a'** 5 μm (applies to **insets a', b'**)

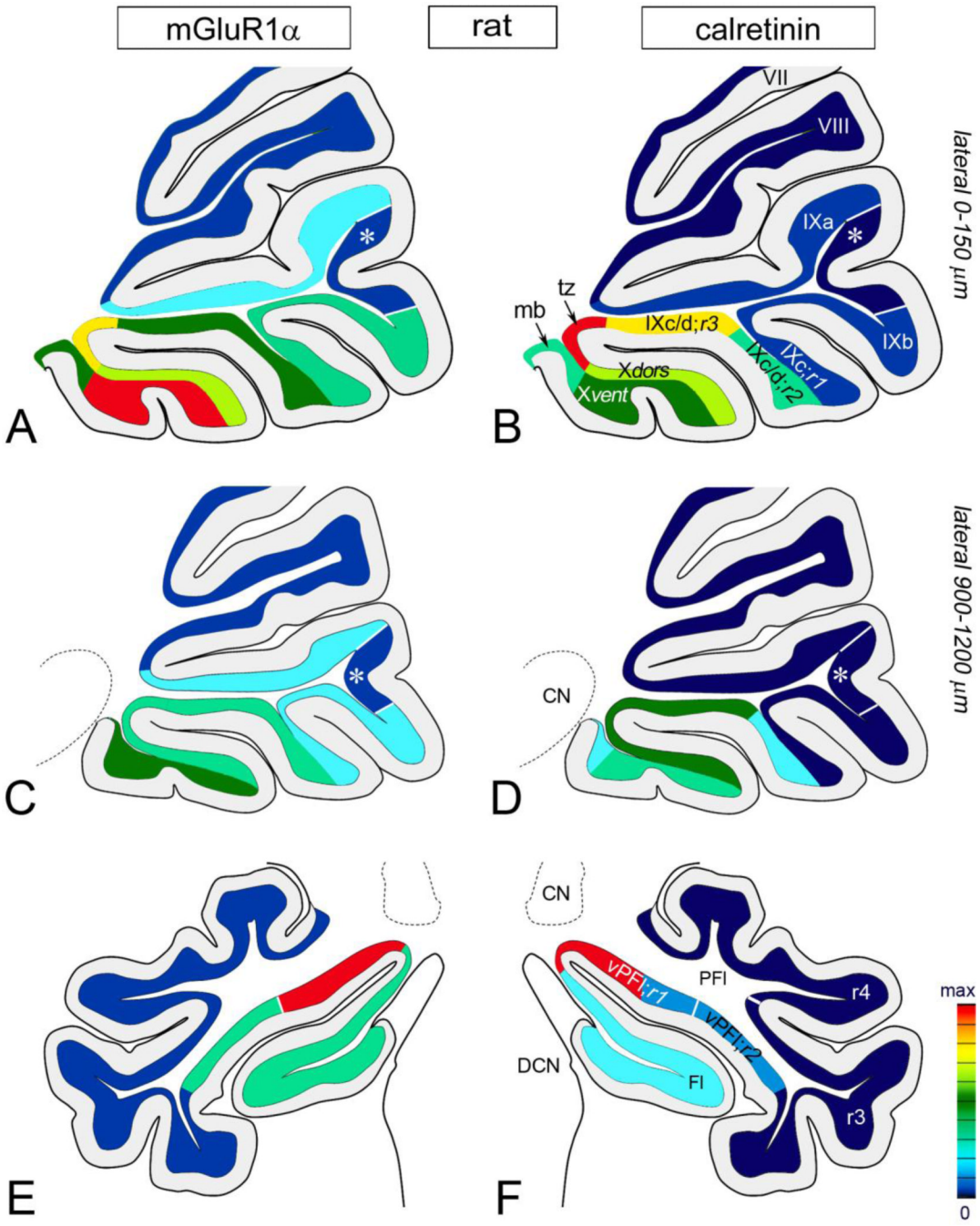

Fig. 8.

A gradient map of UBC subclass distribution in rat cerebellum. The red colored areas represent regions with the highest density (max) of either mGluR1α$^+$ UBCs (**a, c, e**) or CR$^+$ UBCs (**b, d, f**). The deep blue colored areas contain hardly any UBCs. **a-d** Nodulus, uvula and VIII in parasagittal plane. The highest UBC densities for mGluR1α and CR are detected in the midline sections (**a, b**). In the lateral sections (**c, d**) the UBC densities show a marked decrease, especially in nodulus. Differences in the distribution between the two UBC subclasses are apparent. While every lobule contain mGluR1α$^+$ UBCs (**a, c**), albeit with different densities, the CR$^+$ UBCs (**b, d**) are restricted to nodulus and IXc/d;r2&3. The areas

with the highest mGluR1α$^+$ UBC and CR$^+$ UBC densities area the Xvent (**a**) and the tz IX to X, respectively. Asterisk marks a sparse mGluR1α$^+$/CR$^+$ UBC area between IXa and IXb. **e, f** Fl and PFL in coronal plane. Both UBC subclasses are present in high density in the vPFl;r1. The mGluR1α$^+$ UBC are more widespread in PFl than the CR$^+$ UBCs (compare **e** to **f**). For numerical data of UBC densities see Supplementary Tables 2 and 3.

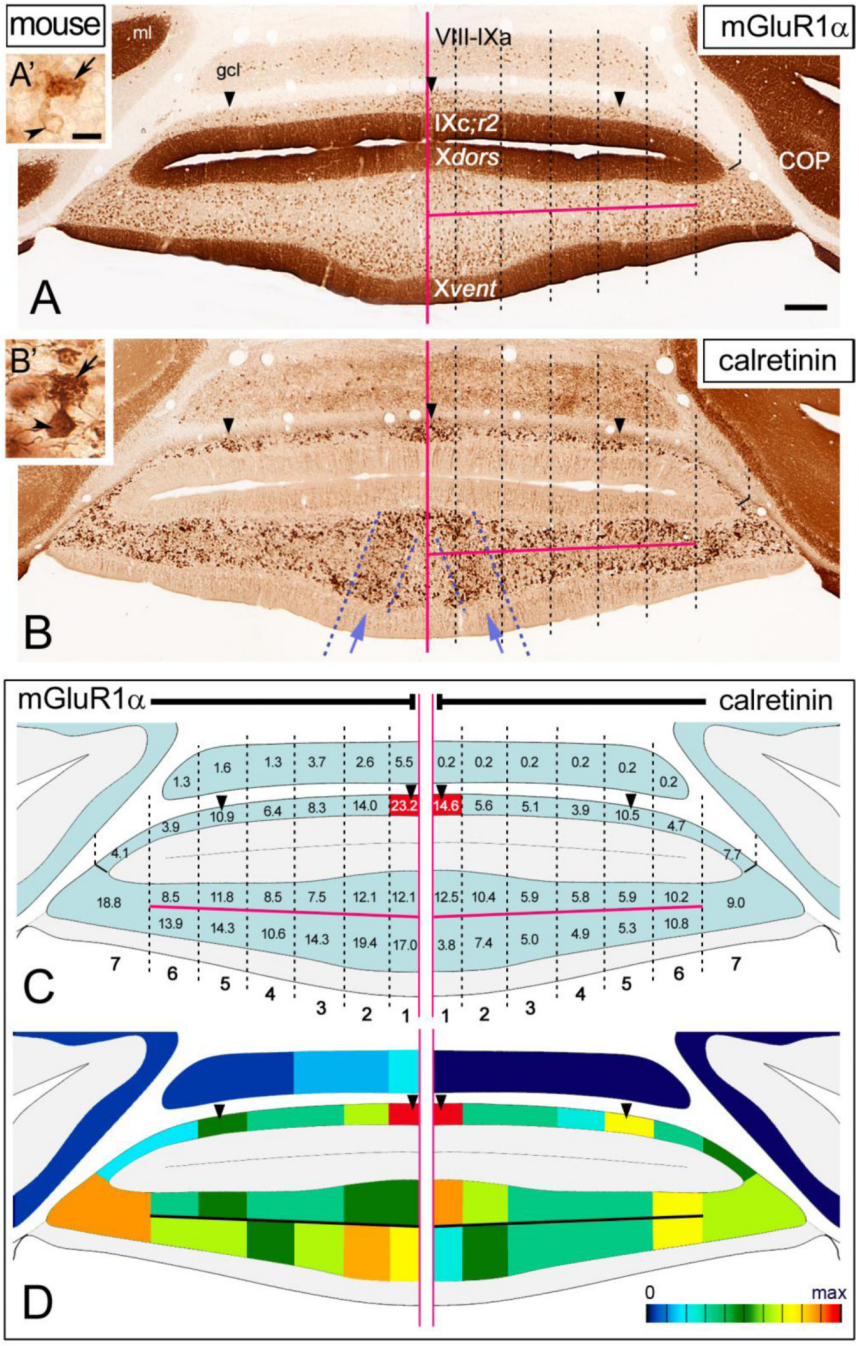

Fig. 9.

Distribution of mGluR1α$^+$ UBCs and CR$^+$ UBCs in mouse nodulus and uvula as seen in coronal sections. The midline of each section is indicated with horizontal magenta colored line. Mid-to lateral zones 1-7 are marked with black dashed lines. Arrowheads indicate UBC rich bands in IXc/d;r2. **a** Typical mGluR1α immunolabeling; intense immunolabeling of Purkinje cell dendrites in ml and distinct immunopositivity in UBCs scattered throughout the gcl, especially in nodulus and IXc/d;r2. The midline zone 1 of IXc/d;r2 shows the highest UBC density, while the midline zones 1, 2 of Xvent and the lateral zones 6, 7 of vermis also contains dense mGluR1α$^+$ UBC population. **Inset a'** shows a representative mGluR1α$^+$ UBC; intense staining in the brush (arrow) and subtle immunopositivity in soma

(arrowhead). **b** Typical CR immunolabeling in UBCs and granule cells. The granule cells somata in gcl and their axons (parallel fibers) in the ml show intense immunopositivity in all cerebellar lobules (VIII/IXa and COP shown) except the nodulus and IXc;r2. These later structures contain a dense CR^+ UBC population and CR^+ mossy fibers. Purple dash line delineate an area (purple arrows) with notably dense population of CR labeled UBCs and mossy fibers. **Inset b'** shows a representative CR^+ UBC; intense staining in the brush (arrow) and cell body (arrowhead). **c** Schematic illustration of the CR^+ (right side) UBC and mGluR1α^+ UBC (left side) distributions in mid-to-later zones. Numbers indicate the density of UBCs (N/0.01mm^2; for standard deviations see Supplementary Table 1). Midline zone 1 in IXc;r2 contains the highest density of both CR^+ UBCs and mGluR1α^+ UBCs (red colored zone). **d** A gradient map illustrates the distribution of UBC subclasses; CR^+ (right side) and mGluR1α^+ (left side). Red color is assigned to the highest cell density (max) of either CR^+ UBCs or mGluR1α^+ UBCs. The deep blue colored area contain hardly any UBCs. *Scale bars* **a** 200 μm (applies to **a-d**), **inset a'** 10 μm (applies to **insets a', b'**)

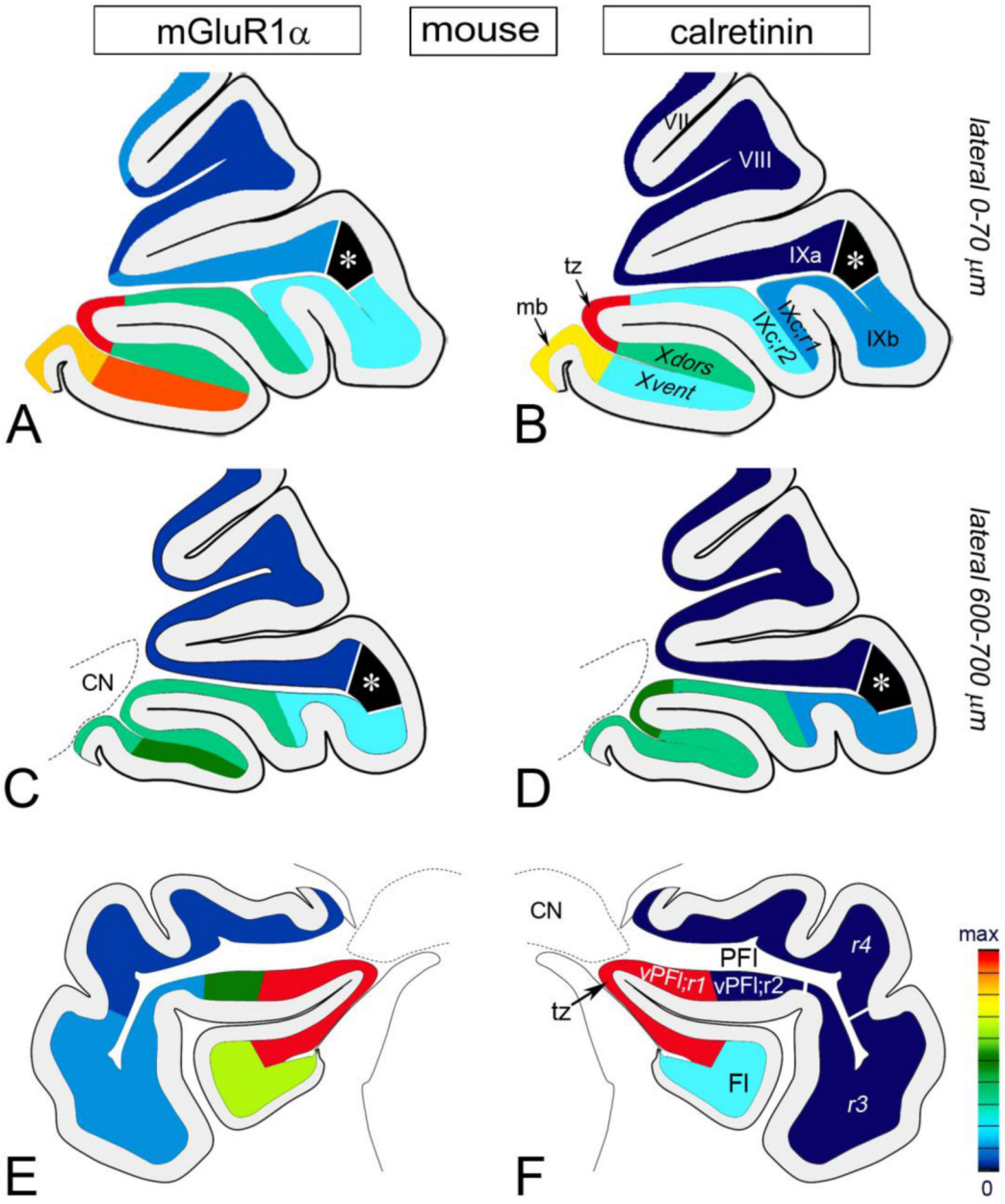

Fig. 10.

A gradient map of UBC subclass distribution in mouse cerebellum. The red colored areas represent regions with the highest density (max) of either mGluR1α$^+$ UBCs (**a, c, e**) or CR$^+$ UBCs (**b, d, f**). The deep blue colored area contain hardly any UBCs. **a-d** Nodulus, uvula and VIII in parasagittal plane. The highest UBC densities for mGluR1α and CR are detected in the midline sections (**a, b**). In the lateral sections (**c, d**) the UBC densities are decreased. The tz IX to X contain the highest density of both UBC subtypes (**a, b**). Differences in the distribution between the two UBC subclasses are apparent, especially in ventral leaflet of nodulus. In Xvent dense mGluR1α$^+$ UBC population is contrasted with low density of CR$^+$ UBCs. While every lobule contain mGluR1α$^+$ UBCs (**a, c**), albeit with different density, the CR$^+$ UBCs (**b, d**) are present mostly in nodulus and IXc;r2. Asterisk marks a distinct field of uvula (between IXa and IXb) that is devoid of mGluR1α$^+$ UBCs and CR$^+$ UBCs. **e, f** Fl and

PFL in coronal plane. mGluR1α$^+$ UBCs and CR$^+$ UBCs are present in high density in the tz Fl to PFl that also includes vPFl;r1. Notably, mGluR1α$^+$ UBC are widespread in PFl but not the CR$^+$ UBCs (compare **e** to **f**). For numerical data of UBC densities see Supplementary Tables 2 and 3.

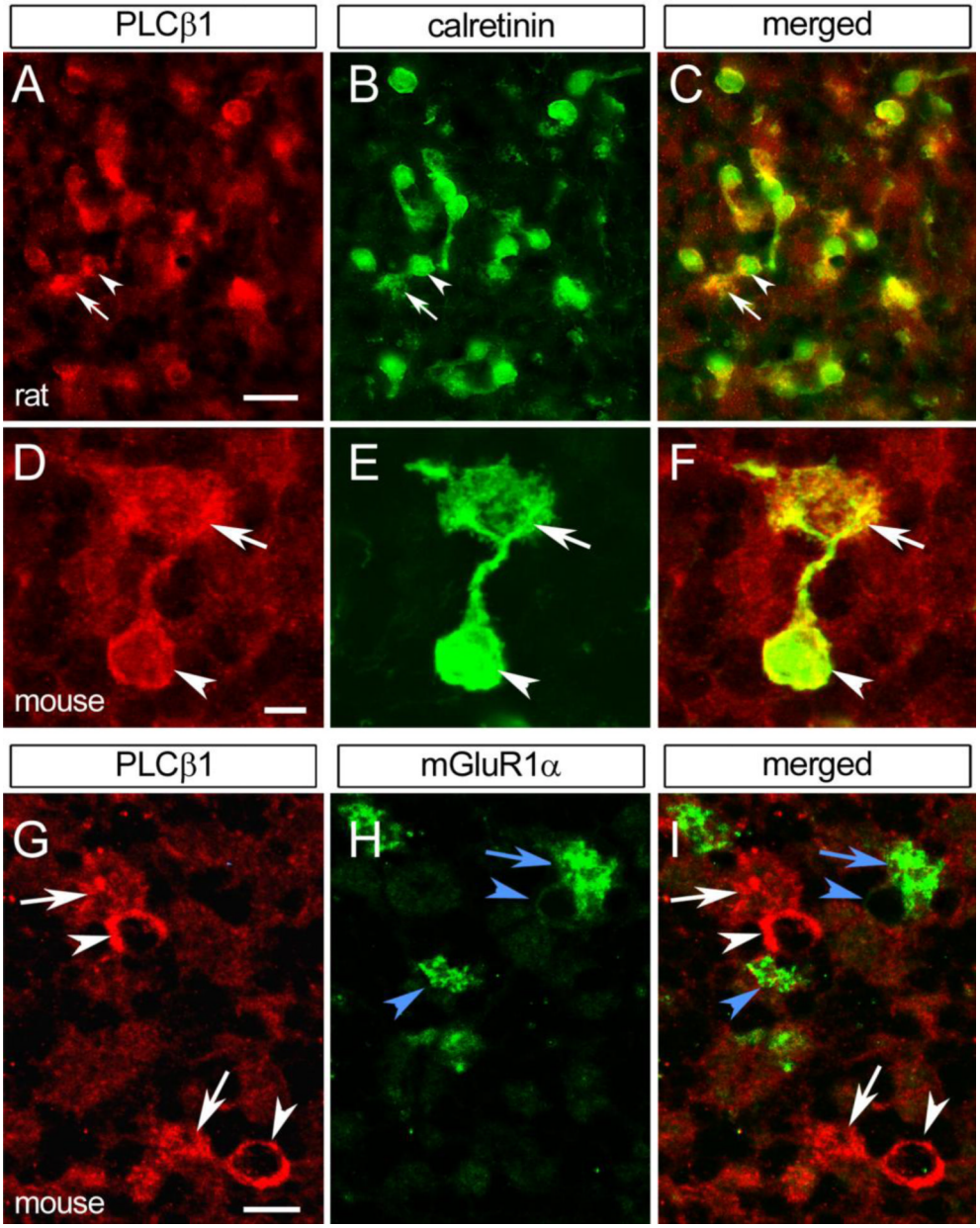

Fig. 11.

Confocal immunofluorescence images of rat (**a-c**) and mouse (**d-i**) cerebellar cryosections from nodulus double-labeled with antisera to PLCβ1 and UBC subclass specific markers. In both species, PLCβ1^{+} UBCs are CR^{+} (**a-f**), but mGluR1α^{-} (**g-i**). White arrows and arrowheads indicate brushes and somata of PLCβ1^{+}/CR^{+} UBCs (**a-g, i**). Blue arrows and arrowheads indicate brushes and somata of PLCβ1^{-}/mGluR1α^{+} UBCs (**h, i**). *Scale bars* **a-c** 20 μm, **d-f** 5 μm, **g-l** 10 μm

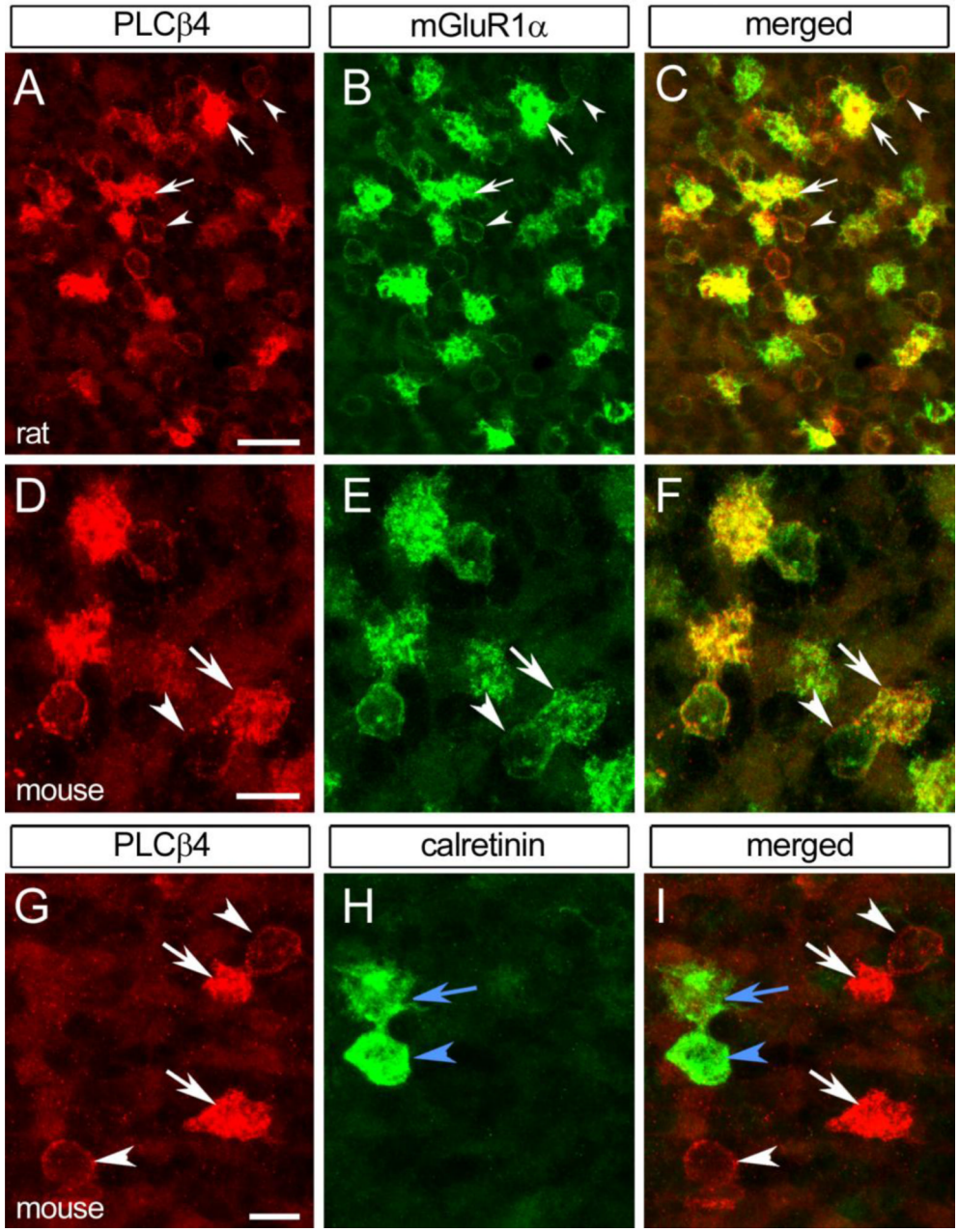

Fig. 12.

Confocal immunofluorescence images of rat (**a-c**) and mouse (**d-i**) cerebellar cryosections from nodulus double-labeled with antibodies to PLCβ4 and UBC subclass specific markers. In both species PLCβ4$^+$ UBCs are mGluR1α$^+$ (**a-f**) but CR$^-$ (**g-i**). White arrows and arrowheads indicate brushes and somata of PLCβ1$^+$/mGluR1α$^+$ UBCs (**a-g, i**). Blue arrows and arrowheads indicate brushes and somata of PLCβ1$^-$/CR$^+$ UBCs (**h, i**). Panels **d-f** are from Tg(Grp-EGFP)DV197Gsat mice; UBC somata show an enhanced signal due to the presence of EGF (**e**). *Scale bars* **a** 10 μm (applies to **a-c**), **d** 20 μm (applies to **d-f**), **g** 20 μm (applies to **g-i**)

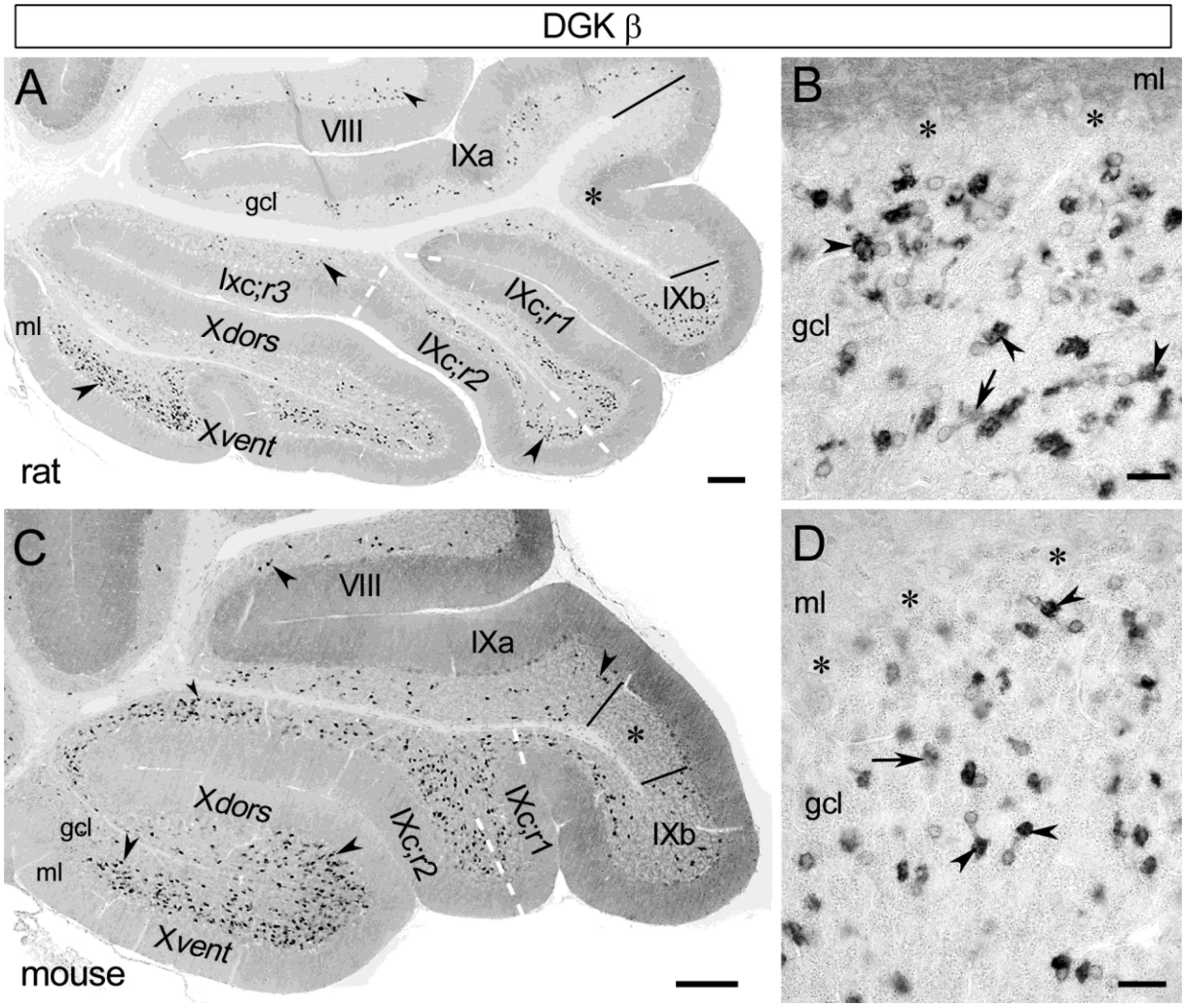

Fig. 13.

DGKβ-immunostaining of paraffin sections of rat (**a, b**) and mouse (**c, d**) cerebella subjected to antigen retrieval; DAB chromogen. **a** Rat parasagittal section illustrates the distribution DGKβ$^+$ UBCs in nodulus and uvula. The Xvent contains the highest density of DGKβ$^+$ UBCs, but IXc;r1-3 and IXb also contain large DGKβ$^+$ UBC clusters. Fewer DGKβ$^+$ UBCs occur in IXa and VIII. Asterisk marks an area (delineated by black lines) with low DGKβ$^+$ UBC density between IXa and IXb. **b** Detail shows groups of DGKβ$^+$ UBC population in rat nodulus with intensely (arrowheads) and moderately (arrows) stained brushes. Asterisks indicate Purkinje cell somata. **c** Parasagittal section illustrates the distribution DGKβ$^+$ UBCs in nodulus and uvula. Nodulus, IXc;r1&2 and IXb contain the highest densities of DGKβ$^+$ UBCs. Fewer DGKβ$^+$ UBCs are present in IXa and VIII. Asterisk marks a distinct field, bordered by lines in uvula, between IXa and IXb, that is devoid of UBCs. **d** Detail of nodulus shows DGKβ$^+$ UBC with intensely (arrowheads) and moderately (arrows) stained brushes (arrowheads). Asterisks in **b** and **d** indicate Purkinje cell somata (**b, d**). *Scale bars* **a, c** 200 μm, **b, d** 25 μm

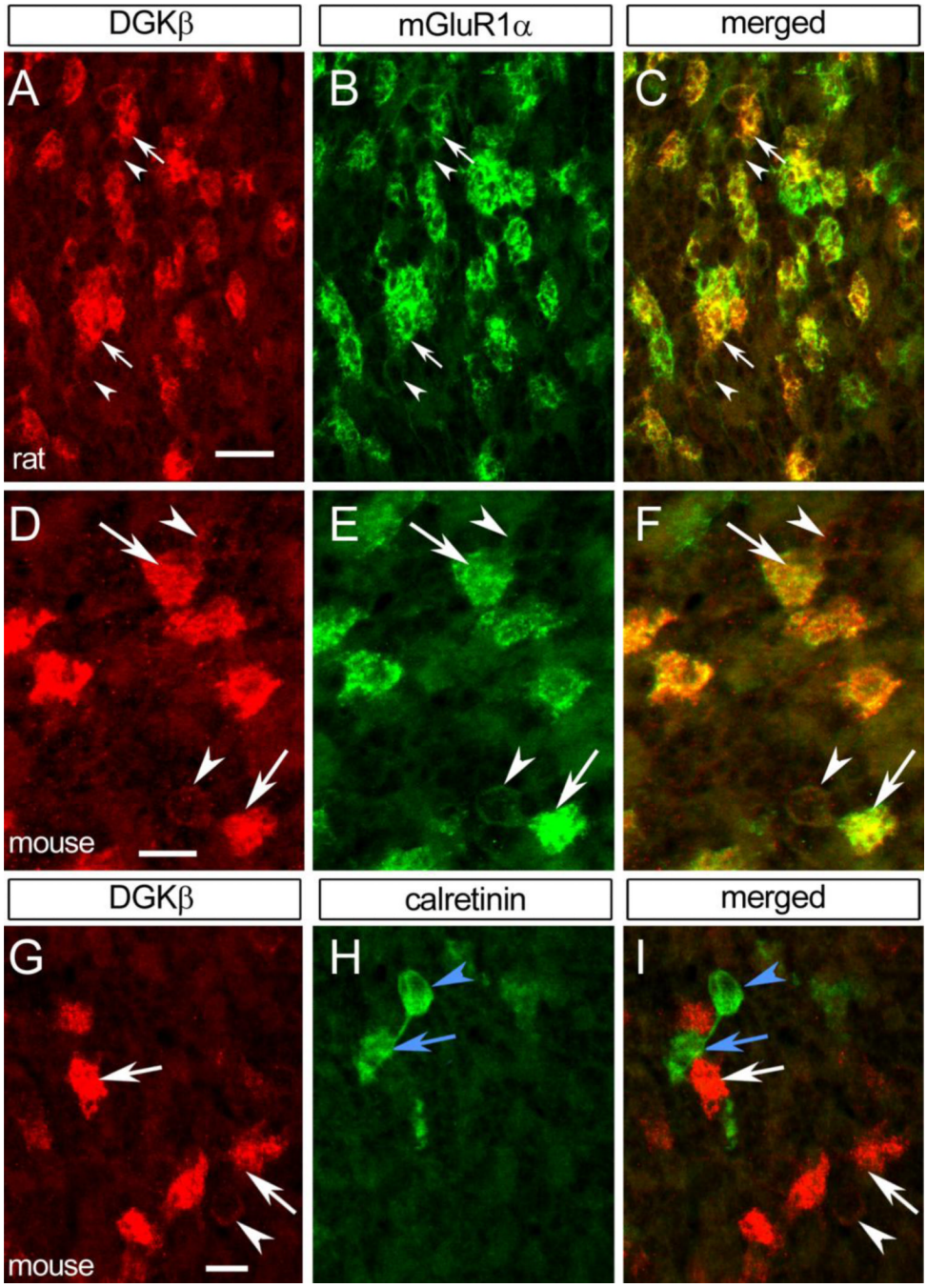

Fig. 14.

Confocal immunofluorescence images of rat (**a-c**) and mouse (**d-i**) cerebellar cryosections double-labeled with antibodies to DGKβ and UBC-subclass specific markers. In both species, DGKβ$^+$ UBCs are mGluR1α$^+$ (**a-f**), but CR$^-$ (**g-i**). White arrows and arrowheads indicate brushes and somata of PLCβ1$^+$/mGluR1α$^+$ UBCs (**a-g, i**). Blue arrows and arrowheads indicate brushes and somata of PLCβ1$^-$/CR$^+$ UBCs (**h**, **i**). *Scale bars* **a** 20 μm (applies to **a-c**), **d** 10 μm (applies to**d-f**), **g** 10 μm (applies to **g-i**)

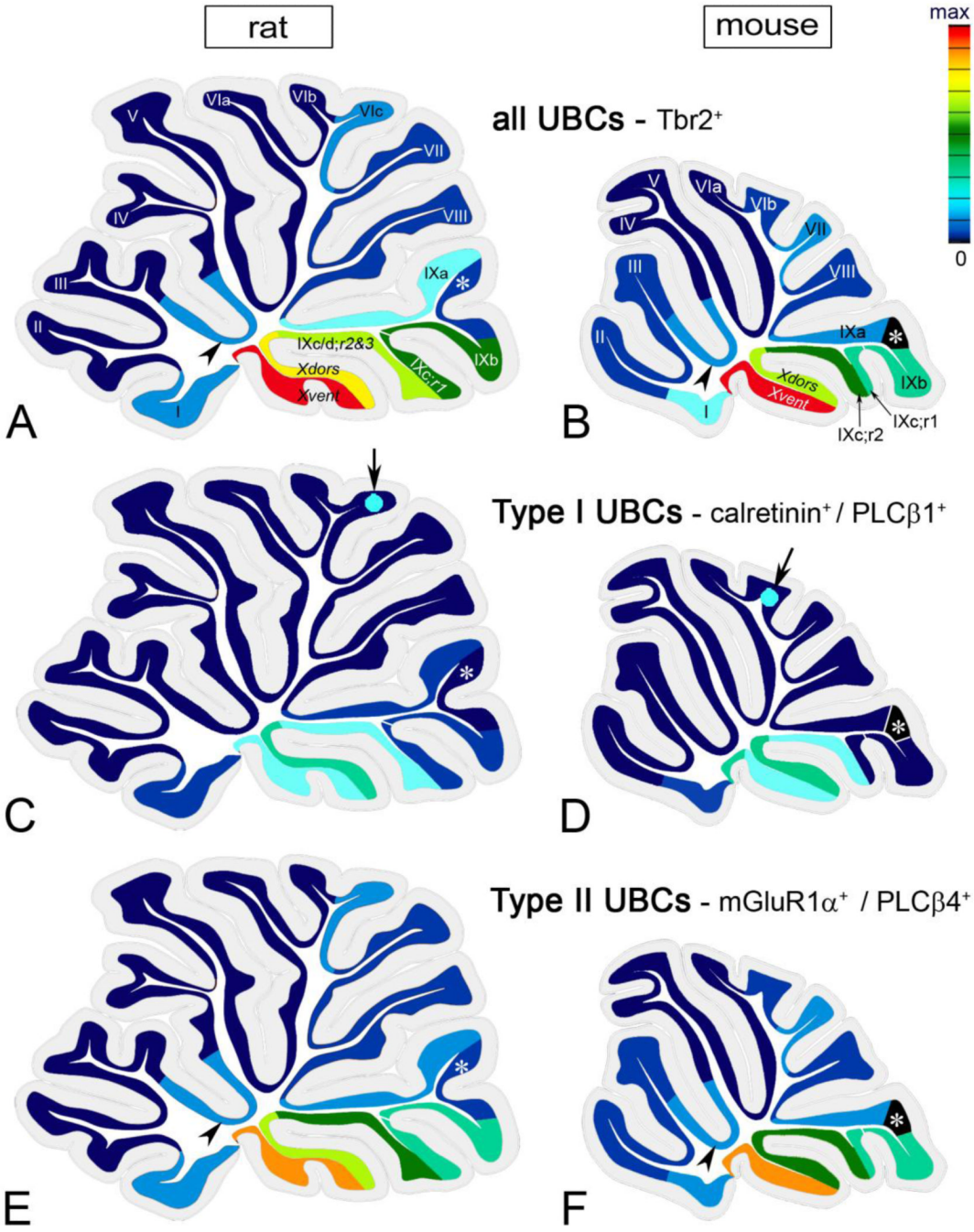

Fig. 15.

A gradient map of UBC distribution in rat (**a, c, e**) and mouse (**b, d, f**) cerebella. A parasagittal section from midline is illustrated. The red colored areas represent regions with the highest density (max) of UBCs. The deep blue colored area contain hardly any UBCs. **a, b** Distribution of all UBCs based on Tbr2 immunolabeling. In both species dense UBC population is associated with the vestibulocerebellum; the Xvent contained the highest UBC density. **c, d** Distribution of type I UBCs based on CR immunostaining. The distribution is shown in proportion to the total Tbr2^{+} UBC number. Type I UBCs are constrained to nodulus and ventral uvula (IXc/d;r2&3 in rat and IXc;r2 in mouse). In both species few type I UBC are present in the lingula; in rat also in the rest of the uvula. Arrows points to areas

with moderate type I UBCs density in VI. **e, f** Distribution of type II UBCs based on mGluR1α$^+$ immunostaining. The distribution is shown in proportion to the total Tbr2$^+$ UBC number. The type II UBCs are more widespread then the type I UBCs (compare panel **e** and **f** to panel **c** and **d**, respectively). They are present not only in nodulus and ventral uvula (IXc/d;r2&3 in rat and IXc;r2 in mouse) but in many other lobules, including the lingula and the rest of the uvula. In both species type II UBCs are rare in IV, V and VIa. Asterisk mark a distinct area in uvula between IXa and IXb. In rat the number of UBC is significantly decreased in this area, especially when compared to the surrounding areas (**a, c, e**). In mouse this area is completely void of UBCs (**b, d, f**). Arrowheads (**a, b, e, f**) point to the tz III to IV that usually contains several type II, but not type I UBCs.

Table 1

List of primary antibodies used in this study

Antibody	Species	Dilution	Specificity	Source	Characterization
Calretinin	mouse	1:2000	full-length recombinant human CR	Swant, Bellinzona, Switzerland	Nunzi et al. 2002
Calretinin	rabbit	1:5000	full-length recombinant human CR	Swant, Bellinzona, Switzerland	Nunzi et al. 2002
DGKβ	rabbit	1 μg/ml	N-terminal region of rat DGKβ	gift of Dr. K. Goto, Yamagata University School of Medicine, Japan	Hozumi et al. 2008
mGluR1α	mouse	1:800	fusion protein containing sequences from C-terminus of rat mGluR1α	Pharmingen	Nunzi and Mugnaini 2009
mGluR1α	rabbit	1:500	peptide representing amino acid residues 945-1127 of mouse mGluR1α	Frontier Institute Co, Japan	Tanaka et al. 2000
mGluR1α	rabbit	1:2500	intracellular C-terminal residues 859–1199 of mGluR1α	gift of Dr. R. Shigemoto, National Institute for Physiological Sciences, Okazaki, Japan	Shigemoto et al. 1997
PLCβ1 G-12 (sc205; lot E040)	rabbit	1:400	peptide mapping at the C-terminus of bovine PLCβl	Santa Cruz	[1]Western blot
PLCβ1 R-233 (sc0905; lot L008)	rabbit	1:400	amino acids 831-1063 mapping within an internal region of rat PLCβl	Santa Cruz	[1]Western blot
PLCβ3	guinea pig	1 μg/ml	C-terminus (amino acid residues 1201-1234) of the mouse PLCβ3	Frontier Institute Co., Japan	Nomura et al. 2007 [2]Western blot
PLCβ3 C-20 (sc403; lot J1811)	rabbit	1:500	peptide mapping near the C-terminus of rat PLCβ3	Santa Cruz	[3]Western blot
PLCβ3 H-84 (sc13958; lot C1710)	rabbit	1:500	amino acids1151-1234 mapping at the C-terminus of human PLCβ3	Santa Cruz	Sarna et al. 2006 [4]Western blot
PLCβ4	rabbit	0.5 μg/ml	amino acids 15-74 of the mouse PLCβ4	Dr. M. Watanabe,	Nakamura et al. 2004
PLCβ4	guinea pig	0.5 μg/ml	amino acids 15-74 of the mouse PLCβ4	Dr. M. Watanabe,	Nakamura et al. 2004
Tbr2	chicken	1:400	KHL-conjugated linear peptide corresponding to mouse Tbr2	Millipore	

[1]Both PLCβ1 antibodies labeled a single band at ~145-150 kDa position (see Fig. 1a).

[2]The PLCβ3 antibody purchased from Frontier Institute recognized a single band at ~175 kDa protein but only in mouse (not shown). This antibody was previously shown to be specific for mouse brain tissue.

[3]The PLCβ3 C-20 (sc403) recognized a single band at ~175 kDa (not shown) in both species. In rat but not in mouse this antibody intensely immunolabed mossy fibers in the granule cell layer and climbing fibers in the molecular layer (not shown). In rat the Purkinje cells showed insufficient, faint immunolabeling. In mouse the antibody immunolabed Purkinje cells, but also crossreacted with other large neurons of the brainstem (not shown).

[4]The PLCβ3 H-84 (sc13958) labeled several nonspecific bands on the blot; particularly a band at ~250 KDa which was more intensely labeled than the 175 kDa PLCβ3 specific band (not shown). In rat and mouse brain sections the PLCβ3 H-84 antibody intensely labeled the endoplasmatic reticuli of most neurons. In mouse the Purkinje cell somata and dendrites were at best moderately labeled; we should however note, that the Purkinje cell immunolabeling pattern was comparable to the one we observed with the guinea pig anti PLCβ3 antibody (Frontier Institute). In rat the Purkinje cells were barely

labeled, just above the background level. Notably, PLCβ3 H-84 was previously used to label murine cerebellar Purkinje cells (Sarna et al. 2006); the difference between our results and the previously published data might be due to differences in the antibody lots sold by the supplier.

Table 2

Expression of PLCβ isoforms in the cerebellar cortex.

		Purkinje cells	UBCs	granule cells	stellate/basket cells	Golgi cells	references
Rat	PLCβ1	++ [1]	+++ type I	++	++	-	Vitale *et al.*, 2004
	PLCβ2						No data
	PLCβ3	++++/++ /- on-off bands	-	-	-	-	Tanaka and Kondo, 1994
	PLCβ4	++++ /++ /- on-off bands	++++ type II	+	-	-	Tanaka and Kondo, 1994; Roustan *et al.*, 1995; Min *et al.*, 2000
Mouse	PLCβ1	+++/+ [2]	++ type I	++	++	-	Watanabe *et al.*, 1998; Hashimoto *et al.*, 2001; Fukaya *et al.*, 2008; Montaña *et al.*, 2012
	PLCβ2	-	-	-	-	-	Watanabe *et al.*, 1998; Hashimoto *et al.*, 2001
	PLCβ3	++++ /++ /- on-off bands	-	-	-	-	Watanabe *et al.*, 1998; Hashimoto *et al.*, 2001; Sarna *et al.*, 2006
	PLCβ4	++++ /++ /- on-off bands	++++ type II	++	-	-	Watanabe *et al.*, 1998; Hashimoto *et al.*, 2001; Sarna *et al.*, 2006; Chung *et al.*, 2009a, 2009b

[1] only the peripheral dendrites are immunolabeled.

[2] all Purkinje cells are PLCβ1 immunolabeled, however they show distinct compartmentalization with moderately and lightly stained bands in the molecular layer

Table 3

Densities (N /0.01 mm^2) of $Tbr2^+$, $mGluR1\alpha^+$ and $calretinin^+$ UBC in 25 μm-thick sagittal cerebellar sections.

	Cerebellar lobules	Calretinin$^+$ (type I)	mGluR1α$^+$ (type II)	Tbr2$^+$ (all UBCs)
Mouse	I-VIII	0.1 ± 0.1	1.4 ± 0.2	1.5 ± 0.1
N=2	IX	2.2 ± 1.6	5.5 ± 0.7	6.4 ± 1.8
	X	6.3 ± 2.1	17.3 ± 2.8	24.6 ± 3.1
Rat	I-VIII	0.3 ± 0.1	0.8 ± 0.05	1.1 ± 0.3
N=2	IX	2.1 ± 0.5	6.0 ± 0.5	8.3 ± 1.6
	X	5.9 ± 0.6	16.4 ± 0.6	20.5 ± 2.2